Building and Environment 209 (2022) 108650

Contents lists available at ScienceDirect

Building and Environment

journal homepage: www.elsevier.com/locate/buildenv

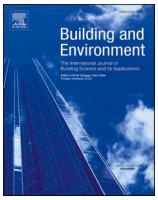

Switching daylight: Performance prediction of climate adaptive ETFE foil façades

Jan-Frederik Flor *, Xiao Liu, Yanyi Sun, Paolo Beccarelli, John Chilton, Yupeng Wu

Department of Architecture and Built Environment, Faculty of Engineering, The University of Nottingham, Innovation Park, Nottingham, NG7 2TU, UK

ARTICLE INFO

Keywords:
Daylight simulation
Bidirectional-scattering-distribution-function
Ethylene-tetrafluoroethylene (ETFE)
Double-skin façade
Responsive architecture

ABSTRACT

This paper reports on the daylighting performance of switchable ethylene-tetrafluoroethylene (ETFE) foil in double-skin façades (DSF). In contrast to conventional glazing or static ETFE façades, switchable ETFE moderates incident daylight and controls internal light distribution by actively responding to weather conditions and solar light intensity. To better understand the light control function of ETFE and the impact of parameters such as climate, latitude and window-to-wall ratios (WWR), a validated optical model was used to evaluate different DSF designs. ETFE façades were modelled with a Bidirectional-scattering distribution-function (BSDF) and spectral data, obtained from experimental measurements, to accurately represent specular and diffuse light transmittance. Based on the five-phase method, a parametric climate data-driven simulation of an office room with different façade designs was conducted for three climate scenarios (Oceanic, Mediterranean, Sub-Tropical). When employing switchable ETFE in façades with different WWRs (30–90%), an annual increase of useful daylight illuminance (UDI) from 11 to 69% in the range of 500–2000lx was recorded. The calculated glare probability (DGPs) declined 59% in the best-case scenarios, providing working conditions with imperceptible glare for 94% of the scheduled time. Simultaneously, the daylight uniformity ratio (UR) increased up to 19% compared to a room with a conventional double-glazed façade. Significant improvements of daylight quality were achieved for façades with large windows in climates with abundant solar light available all year long. Overall, this study contributes to expanding the knowledge on adaptive membrane façades, demonstrating their capacity to enhance the daylighting performance of indoor spaces in different climates.

1. Introduction

1.1. Opportunities and challenges for daylight optimization in buildings with ETFE

Providing sufficient natural daylighting in buildings is essential for enhancing user comfort and reducing energy consumption. Literature suggests that access to daylight could substantially improve building occupants' well-being and productivity while reducing at the same time energy demand for artificial lighting [1]. For the same reason, buildings with better daylighting are also financially more attractive, as suggested in a recent study on the economic value of high-rise real estate, finding rent prices 5–6% higher for spaces with good daylight [2]. It is estimated that artificial lighting in buildings accounts for approximately 15–20% of the global electric energy consumption [3] and 25–40% of the total energy consumption in commercial buildings [4]. Studies have shown that fenestration type and size significantly impact a building's overall energy consumption [5,6]. New buildings offer the opportunity to incorporate design considerations for sufficient natural daylighting provision and create synergetic effects to reduce energy consumption. However, retrofitting windows and shading devices of outdated buildings to improve the internal daylighting conditions is often limited by multiple factors. Old buildings are usually unsuitable for major changes due to structural limitations, or modifications costs are too high [7]. Demolition and new construction are preferred in most cases, adding to the energy and material consumption. Instead, retrofitting and upgrading would extend the building's lifecycle and reduce the CO_2 emission of the building sector [8,9].

Adding an external membrane façade of inflated ETFE foil cushions is proposed in this study, combining lightweight (W = 0.34 kg/m^2), mechanical resistance (TS warp/weft = 64/56 N/50 mm) and high-transparency (T_{vis} = 95%) material characteristics of flexible ETFE foil in a transformative building solution for the enhancement of daylighting performance [10]. This retrofitting measure could improve the

* Corresponding author.
E-mail address: janflor@gmx.de (J.-F. Flor).

https://doi.org/10.1016/j.buildenv.2021.108650
Received 17 August 2021; Received in revised form 15 November 2021; Accepted 2 December 2021
Available online 6 December 2021

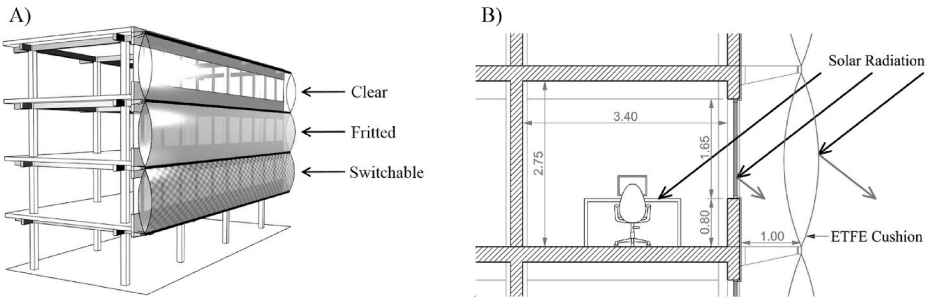

Fig. 1. A) Visualization of a building structure with a double-skin façade with different ETFE foil types. B) Section of a typical single-unit office room with an ETFE double-skin façade and incident solar radiation.

Table 1
Double-skin façade buildings with ETFE.

Project name	Year of completion	Location	ETFE façade type	Switchable
The Shed	2019	New York, US	multi-layer	No
IIT Innovation Center	2018	Chicago, US	multi-layer	yes[a]
US Embassy	2017	London, UK	single-layer	No
Canary Wharf Crossrail Station	2015	London, UK	multi-layer	no
Tic-Media Building	2010	Barcelona, Spain	multi-layer	yes[a]
Unilever Headquarters	2009	Hamburg, Germany	single-layer	no
Centre for Gerontology	2003	Bad Tölz, Germany	single-layer	no

[a] Pneumatical actuation of triple-layer, frit printed ETFE cushion.

building's natural lighting condition with an integrated switchable mechanism adapting to different solar radiation conditions, and potentially also lead to energy savings for heating and cooling due to reduced solar gains and the insulating capacity of multi-layer ETFE [11–15]. A visualization of the building system and a section of an office room with a double-skin façade integrating ETFE foil cushions are shown in Fig. 1A and B.

1.2. Background on ETFE and double-skin façades

ETFE is a fluorine-based polymer with diverse industrial applications. It is frequently used in the form of extruded thin foil (100–300 μm) as an alternative for glass in building construction [16]. Since the erection of the first permanent ETFE foil-covered structure in 1983 in Arnheim, Netherlands [17], ETFE has mostly been employed as a structural or cladding material for canopy coverings of large-scale event facilities. Built examples for the use of ETFE in building façades are encountered less frequently than in roof structures [18,19]. For structural reasons, inflated multi-layer systems are usually preferred over single layer mechanically tensioned systems [20,21].

In recent years, the use of ETFE foil systems has been expanded to a greater variety of building typologies, including educational, commercial and office buildings. However, most projects employing ETFE are still new constructions and only 15.6% account for existing buildings [22]. Within the newly built ETFE constructions, an emerging category using ETFE as a secondary layer of a double-skin façade has become more noticeable over the last decade [23]. This trend seems partly motivated by the demand to reduce the energy consumptions of buildings. Studies show that an external ETFE layer improves the thermal and natural lighting performance of the building envelope and may lead to substantial energy savings [24–29]. Recent research suggests that this might also be true for ETFE with adaptive features [30–32]. An overview of built projects where ETFE has been employed in double-skin façades is provided in Table 1, with examples shown in Fig. 2, A-C.

1.3. Daylight control with switchable ETFE cushions

ETFE has been used previously for daylighting control in buildings [33], mainly due to its capabilities to scatter and evenly distribute light diffusely in space [34–36]. With the increasing number of buildings equipped with ETFE façades, the necessity of understanding the implications on internal daylighting conditions becomes more urgent. Currently, most ETFE buildings are geographically located in the northern latitudes between 50° and 60°. There are significantly fewer in the southern latitudes, with only rare examples in the tropical climate belt [22]. The applicability and benefits of DSF with ETFE for different architectures and climates is currently a question under investigation, and the hypothesis is that the employment of adaptive systems might be a part of the answer [37]. While previous research has mainly focussed on the material performance of ETFE, this study intended to look at the

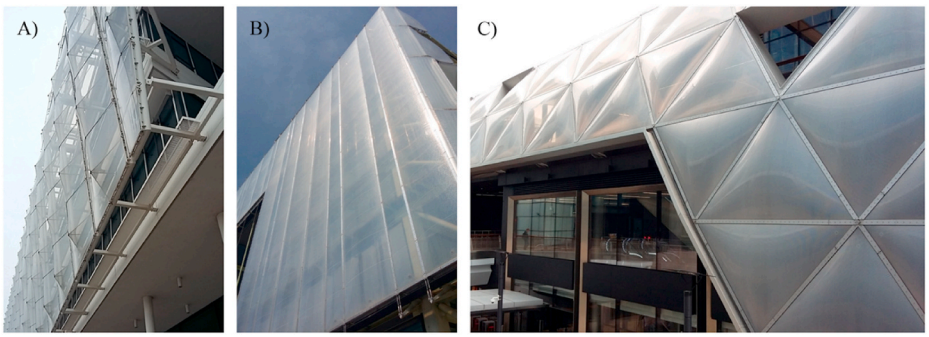

Fig. 2. Double-skin façades with ETFE A) Unilever Headquarter in Hamburg, with single-layer clear ETFE; B) Tic-Media Building in Barcelona with double-layer ETFE cushion in south-west façade, C) Canary Wharf Crossrail Station in London with fritted double-layer ETFE cushion (Pictures by J.-F. Flor, 2016/2017).

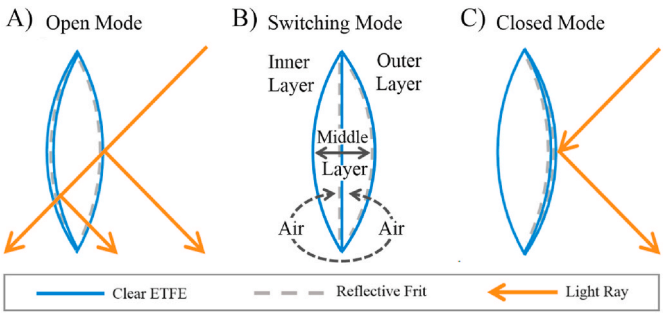

Fig. 3. Light transmittance and reflectance of a switchable ETFE cushion in open (A), switching mode (B) and closed mode (C).

implications of daylighting in architectural spaces. Therefore, an optical model was developed to determine under which parameters ETFE façades, and especially switchable types, deliver adequate daylight performance for well-lit working environments. Fig. 3 A-C shows a schematic section of the adaptive ETFE system investigated in this study.

In contrast to other mechanisms for smart windows, which rely on novel thermochromic or electrochromic materials to achieve the switching effect [38,39], ETFE is a well-established building material proven for large scale applications. With the pneumatic actuation based entirely on mechanical principles, manufacturing, installation and maintenance, as well as control adaptations, are cost-effective and straightforward. The air-inflated ETFE system consists of three layers of transparent foil, with the outer and middle layers printed with a reflective frit pattern [40–42]. The pattern of each layer is shifted to cover the transparent areas of the other when overlapping. The middle layer can be changed from the outer to the inner layer position by injecting air through valves into one or the other air chamber as shown in Fig. 3B and described in Ref. [43]. This process is reversible, allowing the cushion to switch from closed to open mode and back. When the two printed layers are separated from each other, the cushion is in 'open mode' (A), with one part of the incident light passing directly through the cushion while another part is reflected on the outer and middle layer with internal reflections. When the two printed layers are overlapping, the cushion is in 'closed mode' (C), with only a minor part of the incident light passing through the cushion, diffused by the matching frit pattern. In closed mode, most of the incident light is reflected by the reflective print pattern on the cushion's overlapping outer and middle layer. The interplay of specular and diffuse transmission and reflection between the clear and printed parts of the three ETFE layers is complex and further convoluted by the three-dimensional geometry of the pneumatic structure.

1.4. Research aim, objectives and methods rationale

The aim of this study is to understand the daylighting performance of switchable ETFE in a comprehensive way, providing quantifiable performance metrics for different building scenarios and climate conditions. The study's methodological approach uses ray tracing as the primary research method. With the objective to model ETFE double-skin facades realistically for physical accurate daylight simulations, the bidirectional-scattering-distribution-function was used based on spectral data of material samples. Dynamic metrics of useful daylight illuminance, daylight uniformity ratio and glare probability were considered as meaningful dimensions to compare the daylighting performance of different double-skin facades with static and switchable frit prints to conventional double-glazed window façades objectively. The findings are anticipated to make an important contribution to the field of adaptive membrane structures, demonstrating, for the first time, with physics-based simulations, how switchable ETFE in DSFs meet dynamic daylight metrics.

2. Methods

2.1. Overview of the research methodology

The workflow adopted for this daylighting study comprises a combination of experimental and computational methods supported by a network of simulation software. Spectral analysis of ETFE material samples was conducted in a laboratory setup which provided the source data for applying the bi-directional scattering distribution function to generate detailed multi-angled optical models for the daylighting simulation. These were based on the five-phase-method using Radiance software, operated through Honeybee/Ladybug environmental analysis tools and the graphic programming plug-in Grasshopper within the 3D modelling software Rhinoceros [44,45]. Annual weather data and BSDF files were compiled together with the model geometry, calculating hourly illuminance values for a grid of test points. The results were transferred to the 3D environment of Rhinoceros via the controls of Honeybee/Grasshopper for visualization and data post-processing [46,47]. A simplified outline of the described workflow can be seen in Fig. 4. The specific method for each of the above-summarized procedures is described in detail in the following sections.

2.2. Tested ETFE foil

This section describes the methodological steps towards obtaining the optical properties of ETFE foil with switchable print patterns required to generate an optical twin model of the switchable ETFE cushion. Measurement methods, spectral data and overall transmittance and reflectance of ETFE foil are detailed on continuation. Architen Landrell supplied the commercially available foil samples for the tests.

2.2.1. Optical measurement method

The optical characteristics and lighting qualities of ETFE foil have been well covered in the literature [33,48–51]. Considerable variations in the optical characteristics have been reported for different foil types depending on parameters, such as thickness, tint saturation, tint colour, frit ink, print density and area of frit coverage. However, scattered light transmission and reflection is usually not considered, yet it is an

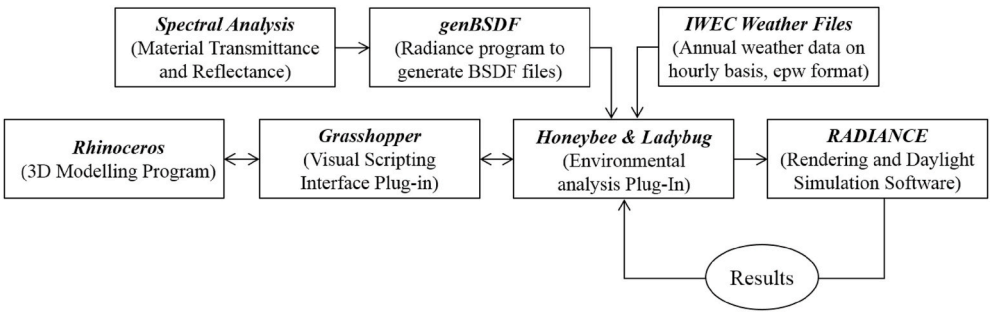

Fig. 4. Workflow diagram for model generation and daylight simulation.

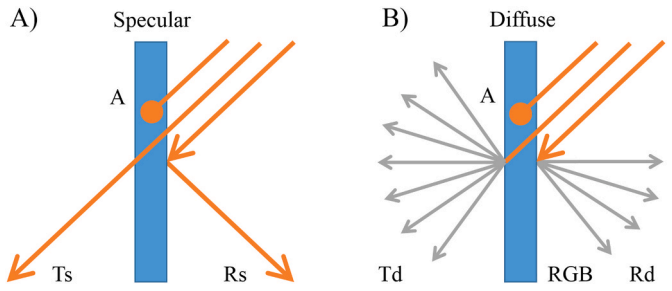

Fig. 5. Specular (A) and diffuse (B) light transmittance and reflectance on a translucent material section.

important aspect of daylighting. In order to accurately predict the daylighting qualities of spaces covered with switchable ETFE, a physics-based model describing the specular and diffuse light transmission and reflection, as depicted in Fig. 5A and B, is necessary.

Due to the lack of data at the required resolution, spectroscopic measurements determining specular and diffuse light transmittance and reflectance of the ETFE material were carried out. These measurements were crucial to generate the BSDF files needed for the annual daylight simulations.

The material sample consisted of a 210 × 297mm sheet of clear 200 μm extruded ETFE foil printed with a silver ink pattern in two densities. The sample's print pattern was composed of a square grid with clear, fritted and densely fritted areas. The spectral transmittance and reflectance of the three surface areas were measured using a calibrated spectrometer USB2000+VIS-NIR-ES (spectral range: 339–1024 nm), a tungsten halogen light source HL-2000, a transmission integrating sphere FOIS-1 and a reflection integrating sphere ISP-REF, supplied from Ocean Optics, as shown in Fig. 6 A/B. The ISP-REF integrating sphere includes a gloss trap on the sphere wall to fully absorb the specular component of reflected light and allow the measurement of the diffuse-only reflectance. When the gloss trap is disabled, the specular component is included, and the integrating sphere performs a total reflectance measurement. The specular reflectance can be calculated by subtracting the diffuse reflectance from the total reflectance. The FOIS-1 integrating sphere is designed for total transmittance spectra acquisition. The specular transmittance can be measured by using a similar setup as in Fig. 6A but with a fibre detector (with a field of view of 0°) instead of the integrating sphere. The details of this method are described in Ref. [52]. Based on the measured total and specular transmittance, the diffuse transmittance can be calculated. A picture of the switchable ETFE sample is shown in Fig. 7.

2.2.2. Optical properties of ETFE foil samples

For the daylight analysis, and hence, for the optical characterization, only the visible light spectrum was considered, following Equation (1) [53]:

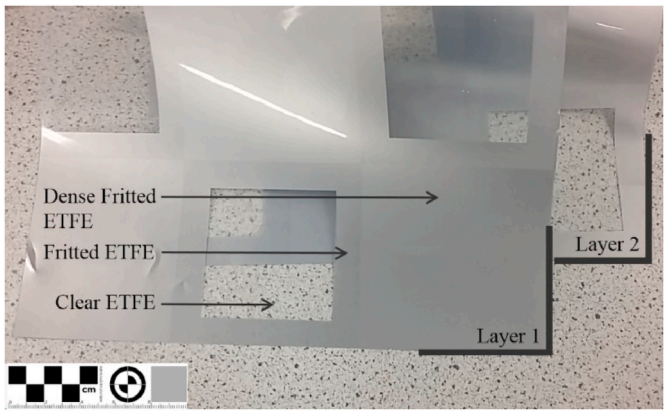

Fig. 7. Two samples of switchable ETFE foil.

$$\tau_v = \frac{\sum_{\lambda=380nm}^{780nm} \tau(\lambda) D_\lambda V(\lambda) \Delta\lambda}{\sum_{\lambda=380nm}^{780nm} D_\lambda V(\lambda) \Delta\lambda} \quad \text{Equation 1}$$

Where D_λ is the relative spectral distribution of illuminant D65, $\tau(\lambda)$ is the spectral transmittance of the material sample, $V(\lambda)$ is the spectral luminous efficiency for photopic vision defining the standard observer, and $\Delta\lambda$ is the wavelength interval. Therefore, the spectral data outputs were trimmed to a useful wavelength range from 380 nm to 780 nm for the subsequent daylight simulations. This was done using Ocean Optics spectrometer operating software OceanView (1.6.7) according to the relative spectral distribution D_λ [53].

The graphs of Fig. 8 A, B, C and D show an overview of the measured specular and diffuse transmittance and reflectance for each material combination on the sample. Data observations show, that all three ETFE surface types have distinct optical characteristics. While the clear ETFE has a high specular transmittance ascending over the spectrum, the diffuse transmittance reduces, according to Fig. 8 B. The opposite is the case for fritted ETFE, showing a low specular transmittance (Fig. 8 A) and approximately doubling for the diffuse light transmittance in comparison to the clear ETFE (Fig. 8 B). The densely fritted ETFE has both the lowest specular and diffuse transmittance values but the highest diffuse reflectance values over the wavelength range.

Based on the spectral measurements, the global, specular and diffuse visible light transmittance T_{vis} and reflectance R_{vis} were calculated according to BS EN 410 [54]. The visible light absorbance A_{vis} was derived using the calculated global visible light transmittance and reflectance according to the law of energy conservation: $T_{vis} + A_{vis} + R_{vis} = 100\%$ [55]. Table 2 summarizes the optical characteristics of the tested samples.

Overall, the spectral analysis confirmed the observations reported in the literature about the relatively homogenous light distribution of ETFE across the visible spectrum [56–58]. However, taken together with the results from the specular and diffuse light analysis, it becomes clear that

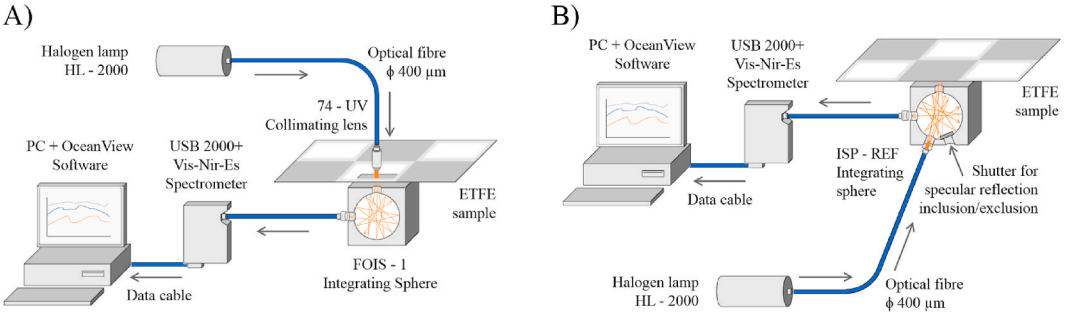

Fig. 6. Experimental setup: A) measurement of specular transmittance and B) specular reflectance.

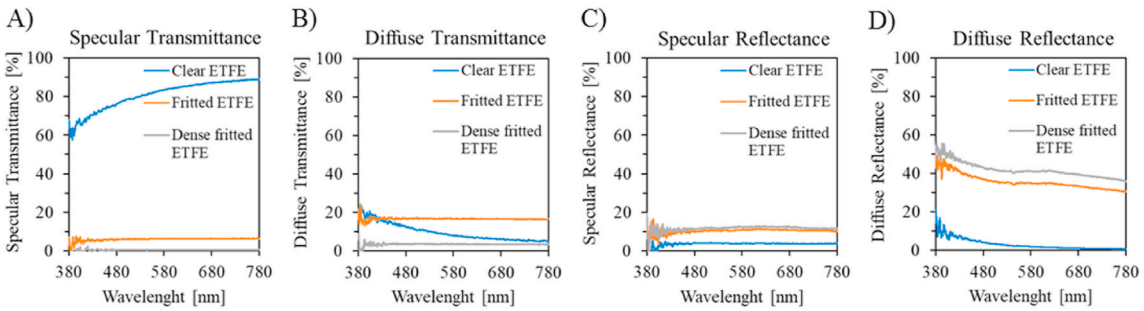

Fig. 8. Spectral distribution of specular transmittance (A), diffuse transmittance (B), specular reflectance (C) and diffuse reflectance (D) of three surfaces (clear, fritted and dense fritted) on switchable ETFE foil.

Table 2
Optical characteristics of visible light transmittance, reflectance and absorbance of three types of surface (clear, fritted and dense fritted) on switchable ETFE, calculated according to BS EN 410 [54].

Foil Type	Global T_{vis}	Global R_{vis}	Specular T_{vis}	Specular R_{vis}	Diffuse T_{vis}	Diffuse R_{vis}	A_{vis}
	[%]	[%]	[%]	[%]	[%]	[%]	[%]
Clear ETFE Foil	91.0	6.2	81.8	3.8	9.2	2.4	2.8
Fritted ETFE Foil	23.0	45.7	6.1	10.6	16.9	35.1	31.3
Dense Fritted ETFE Foil	4.0	53.2	0.4	12.0	3.6	41.3	42.8

light scattering properties play an important role in overall light transmittance of ETFE and, therefore, the daylight distribution in internal spaces. This aspect might have been underestimated in previous studies.

2.3. Modelling of ETFE cushion

The following section describes the generation of an optical model that mirrors a real-size, switchable ETFE cushion mock-up, designed together with Architen Landrell based on previous developments and manufactured in their production facilities to industry specifications. Modelling the ETFE geometry and applying the optical material properties is a preliminary step for generating the BSDF transmission matrix required for the simulation process [59]. The methodical steps described in this section include geometry generation, material modelling, and combining cushion geometry and material definitions.

2.3.1. Cushion geometry

The double-curved geometry of the inflated ETFE cushion was generated using RhinoMembrane V2.0 [60], a Rhinoceros 3D plugin for modelling tensioned membrane structures which is based on the Update Reference Strategy (URS), a generalized derivation of the force density method [61,62]. The form-found geometry of the virtual ETFE cushion mirrored the existing mock-up with analogue dimensions described previously in detail by the authors [43]. The ETFE cushion measured 1000 × 1000mm with a maximum curvature displacement of 10% on each side of the central plane, equating to a 200 mm maximum distance between the layers at the centre of the cushion section. The form-found cushion geometry was meshed and edited to achieve a regularly laid out triangulated mesh distribution, facilitating a smoothed surface for accelerated ray intersection during the daylight simulation [63]. Five models with increasing mesh density, ranging from 200 to 20000 mesh face elements (A-E), were tested for curvature smoothness and mesh face planarity. Fig. 9 shows the five cushion mesh models in plan view.

A mesh independence test was carried out to ensure the accuracy of the shape and subsequent realistic optical behaviour. Beyond 9248 mesh elements, no significant result deviations were found. Therefore, and for the sake of computational economy, model D was chosen as the final mesh geometry. The mesh was then divided into three sub-groups to accommodate the switchable print pattern and facilitate the assignment of the different material definitions.

2.3.2. Material definition

In a second step, Radiance material definitions were generated for the three ETFE sample surfaces (clear, fritted, dense fritted) based on the spectral measurements. Spectral data sets were converted to RGB (red, green, blue) values, a requirement for the daylight simulations input. As a pre-step for obtaining RGB, CIE X, Y, and Z values, representing the emitted light intensity weighted for each wavelength, were calculated [64]. RGB values for the diffuse reflectance were calculated using spectral measurements at a wavelength interval of 10 nm in the range of 380–780 nm, converting spectral data first to XYZ chromaticity coordinates for 2° and 10° of a standard observer and then transforming to RGB values. The CIE chromaticity coordinates were chosen as an appropriate standard for colour spaces of a D65 reference illuminance source since CIE is also used by Radiance software to define the red, green, and blue channels (RGB) of diffused light reflectance [63]. An overview of the calculated RGB values, representing the reflected colour of the material surfaces, is shown in Table 3.

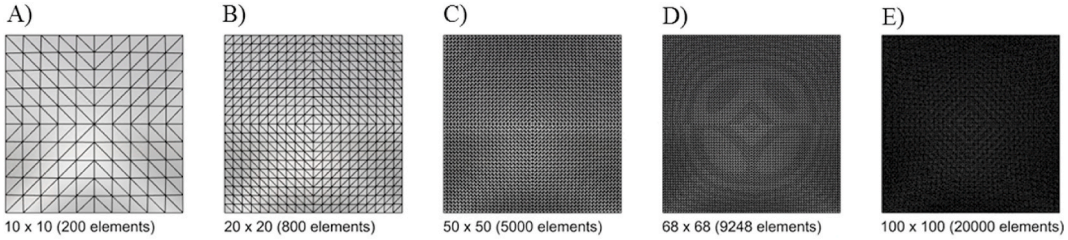

Fig. 9. Modelled cushion geometry with different mesh densities (A–E).

Table 3
Diffuse reflectance values of red, blue and green channels (RGB) for switchable ETFE surface types.

RGB Color Model	Clear ETFE			Fritted ETFE			Dense Fritted ETFE		
	R	*G*	*B*	*R*	*G*	*B*	*R*	*G*	*B*
CIE RGB	33	48	69	157	159	166	169	171	177

Based on the measured specular and diffuse transmittance and reflectance as well as the RGB reflectance values, the ETFE material types were modelled consequently as a Radiance 'trans material'. This material definition was selected as the closest fit to the characteristics of ETFE among the available Radiance material options [63,65]. The generated Radiance material definitions for the three ETFE types that were assigned to the different parts of the cushion geometries are listed below:

```
void trans Clear ETFE
0
0
7 1.000 1.000 1.000 0.038 0.001 0.946 0.899

void trans Fritted ETFE
0
0
7 0.942 0.953 0.999 0.106 0.001 0.270 0.265

void trans Dense Fritted ETFE
0
0
7 0.801 0.806 0.838 0.120 0.000 0.056 0.100
```

2.3.3. Combining cushion geometry with ETFE material

In the following modelling step, the generated ETFE material definitions were assigned to the individual mesh parts of the triple-layer cushion geometry according to the switchable ETFE cushion mock-up design. The meshes of each material and layer were recombined within Radiance to obtain a complete triple-layer cushion model. Fig. 10 shows the generated three-dimensional mesh model of the switchable triple-layer ETFE cushion in perspective, side and front view with all material types colour coded for material assignment.

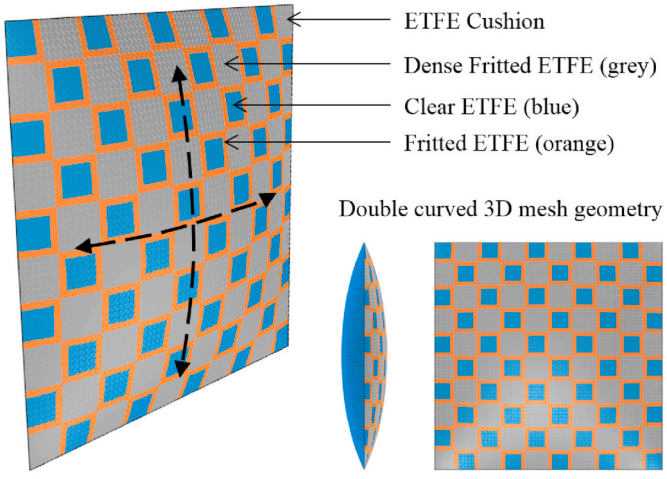

Fig. 10. Cushion geometry (perspective, section and plan view) with colour code mesh divisions for material assignment. (For interpretation of the references to colour in this figure legend, the reader is referred to the Web version of this article.)

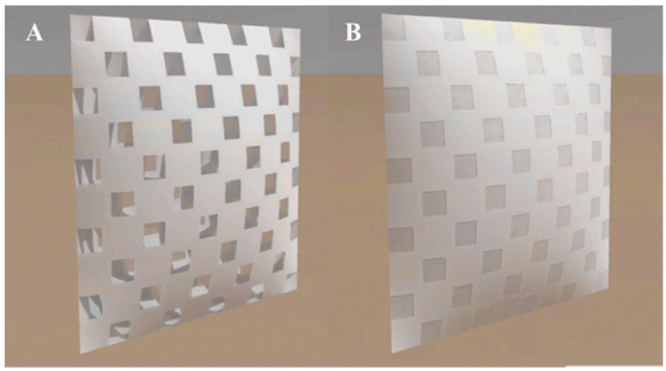

Fig. 11. Photorealistic rendering of switchable ETFE cushion, in open (A) and closed mode (B).

A test rendering of the switchable ETFE cushion in open and closed mode was performed in Radiance with photorealistic image output (2000 × 2000px), shown in Fig. 11. After visual verification of the renderings and comparison with pictures from the mock-up to reconfirm realistic representation of the materials and geometry, the model was exported from the Grasshopper/Honeybee environment to Radiance as separate material and geometry.rad files. Within the Radiance environment, the material and geometry files of the individual layer parts of the ETFE cushion were recombined into one single file for the BSDF processing.

2.4. BSDF of switchable ETFE cushion

This section describes the methods for generating BSDF data for the three-dimensional model of the ETFE cushion and presents the key features of the ETFE BSDF in detail.

2.4.1. Methods for BSDF generation

ETFE is a material with light-diffusing properties, as shown with the spectral analysis, with scattered light being a considerable fraction of the overall material light transmittance [66]. Annual daylight simulations of the optical behaviour require a high degree of computational power to calculate the multiple reflections between different material layers [67]. Therefore, instead of using a complete 3D model of the ETFE for the daylight simulation, which would require ray-tracing calculations of material and geometry for every hour of the year, bidirectional-scattering-distribution-function (BSDF) is employed. BSDF is a mathematical function that describes the light scattering behaviour of optical surfaces [68]. It is used in daylight simulations for solving the angular light transmittance and reflectance of complex fenestration systems, which is pre-calculated and then applied to a simplified proxy geometry within the building model [69–73]. The state-of-the-art methods for generating BSDF of window and façade daylighting systems have been identified recently by the International Energy Agency [74]. However, deriving BSDF of a real size ETFE cushion sample directly with experimental methods using goniophotometry [75] is currently not feasible due to the unavailability and cost of large-scale equipment. Therefore, in this study, computational methods were employed using the Radiance program genBSDF. The virtual generation of BSDF with ray-tracing methods had been validated previously with studies on complex solar screens and other fabric façade materials [76–78]. A workflow diagram showing the main procedure steps for generating the BSDFs of the ETFE DSF is shown below in Fig. 12.

2.4.2. Key features of switchable ETFE's BSDF

BSDFs were generated for the open and closed state of the switchable ETFE cushion and three alternative DSF models with double-glazing and static frit print patterns and clear ETFE. In order to verify values for different incident angles and evaluate the plausibility of the overall

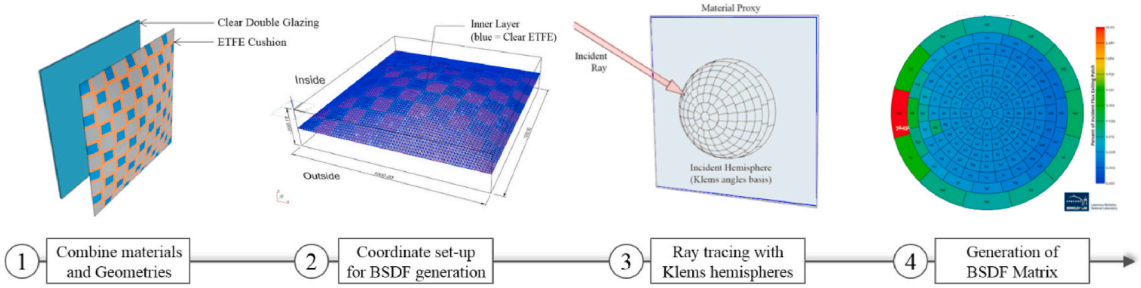

Fig. 12. Workflow diagram for BSDF generation of ETFE cushion and combined DSF.

transmittance and reflectance data, BSDF data files were loaded for visual crosscheck in the BSDFViewer program [70]. Transmission and reflection values for all 145 angles of the Klems hemisphere were plotted on the front- and backside of sample matrixes and examined for individual incidence angles [79]. A selection of the Klems BSDF diagrams with the datasets for specific incidence angles of the open and closed mode is shown in Fig. 13, with distinct transmission patterns observable for both optical states of the model.

The data plots show that the direct hemispherical visible light transmission at the backside side is somewhat lower in closed than in open mode. The overall transmission values in open mode range from 10.5 to 58.2%, and in closed mode, from 4.1 to 57.8%. The lowest transmission values were observed at perpendicular incidence angles and the highest values at lateral incidence angles. The directional scattering effects are more noticeable at incidence angles close to the cushion's horizontal axis, while a more homogenous light transmission is observed for incidence angles close to the vertical cushion axis. Dispersive scattering effects were observed to be more pronounced in the reflected light due to the convex lens shape of the cushion geometry. The plotted BSDF data shows a considerable variation of transmission and reflection for different incidence angles. Therefore, the single incidence angle is only indicative and does not reflect the overall performance of the ETFE cushion, confirming the authors' previous studies on optical aspects and angle-dependent behaviour of ETFE.

2.5. Validation of ETFE model

Radiance programs and daylighting simulations incorporating BSDFs have been validated previously in several studies [65,66,80,81]. However, switchable ETFE cushions with multiple assigned materials have not been assessed before, lacking reference data of ray-tracing simulations for comparison. Therefore, and due to the model's complexity, a validation was carried out to evaluate the reliability of the BSDF model. For this purpose, a test box measuring 1 m × 1 m x 1 m with opaque non-reflective surfaces was built around the switchable ETFE mock-up. The internal illuminance was measured with a DT-8820 illuminance sensor, with an accuracy of ±(5.0% + 10d), at 10 points with 100 mm separation aligned along the centre line section of the box. The measurements were done on the 21st of June at 10 a.m. under cloudy sky conditions with an approximate sky luminance of 10k lx with the ETFE in open mode switch state and a southward orientation. The model and sky conditions were replicated in Radiance, and a point in time simulation of the virtual test box performed using the 5-phase method with the corresponding BSDF file. Fig. 14 shows a picture of the switchable

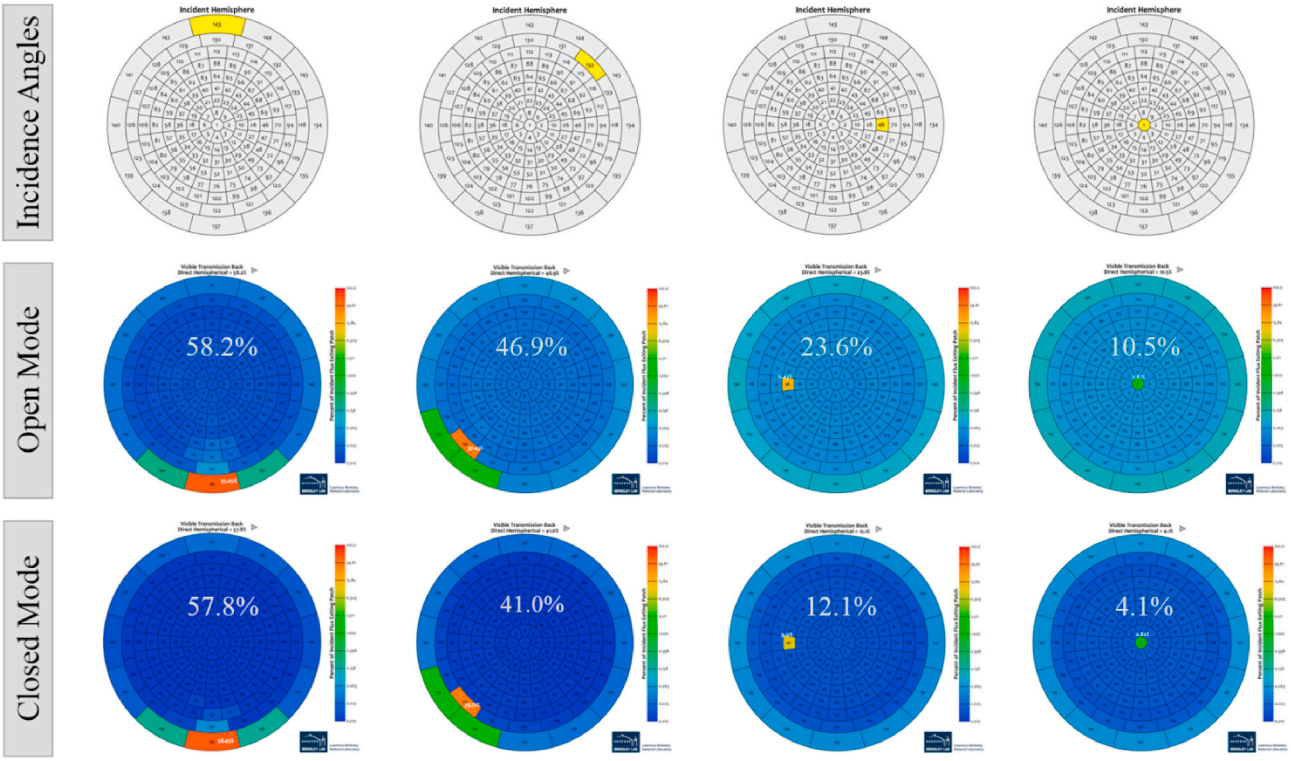

Fig. 13. Selected BSDF plots of switchable ETFE cushion in open and closed mode.

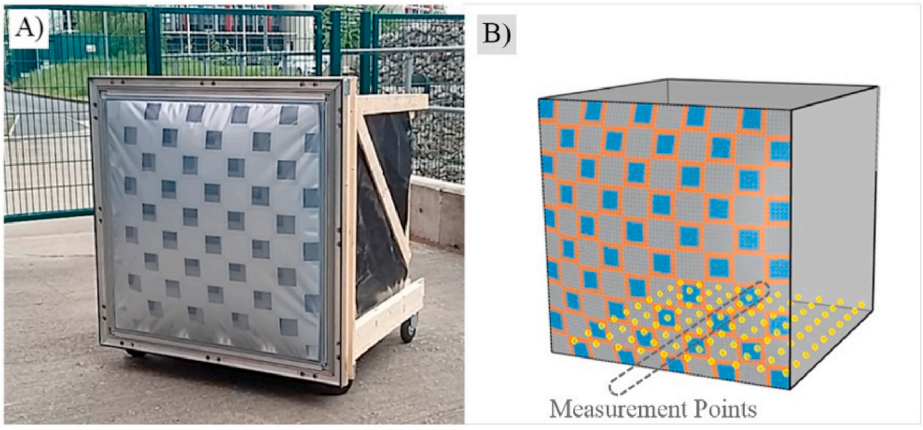

Fig. 14. A) Mock-up of switchable ETFE cushion with a solar shielded test-box; B) virtual-twin model of test-box with measurement points.

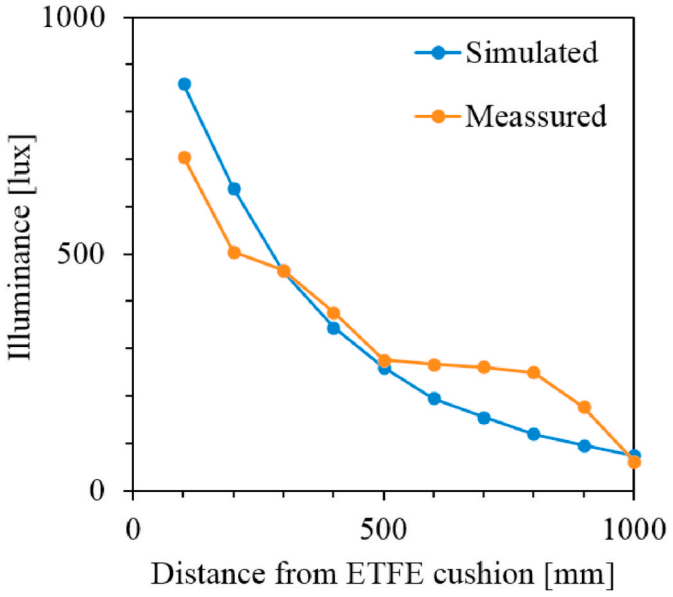

Fig. 15. Comparison of measured and simulated illuminance across the test box section with switchable ETFE cushion in open mode.

ETFE cushion mock-up (A) and an image of the mirrored virtual model with horizontal test points (B).

Overall, the measured illuminance within the mock-up followed a similar trend to the simulated BSDF model, with lower values at the back of the test box and a steep increase towards the opening shown in Fig. 15. The overall mean illuminance for the simulation results agreed well with the measured value with only 4.3% difference. The errors are most likely related to inaccuracies in the illuminance measurements, common in experimental outdoor tests. Variances might have also resulted from the changing solar exposure during the measurements and inaccuracies in placing the sensor horizontally within the test box. Another likely reason might have been internal reflection inside the test box resulting from the black plastic box cover, which is not flat enough and reflects some light toward the back of the box, therefore, causing higher illuminance readings towards the backside of the mock-up box, compared to the simulation model. Despite these uncertainties and limitations, the comparative test results created enough confidence in the BSDF models to proceed with the daylighting simulations.

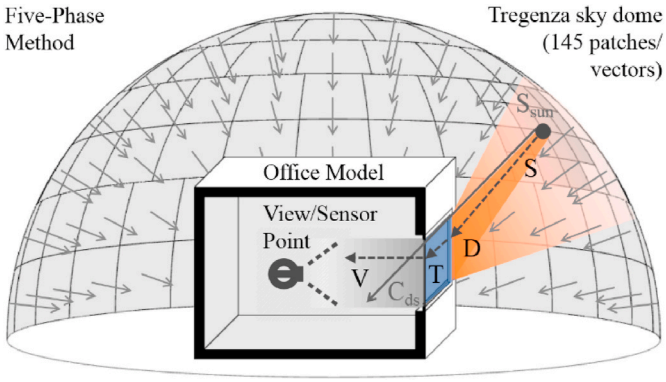

Fig. 16. Five-phase method daylight scene.

2.6. Dynamic daylight simulation method

This section describes the main method and parameters of the daylighting simulation, focussing on the details of the five-phase method, sky model, office geometry, simulation scenarios and parameters, weather data of the chosen locations and the dynamic metrics employed for the analysis of the results.

2.6.1. Five-phase method

The current state of the art method for daylighting simulations is the validated five-phase method, based on backwards ray-tracing [81–83]. This method makes it computationally feasible to simulate the annual daylight performance of complex fenestration systems using bidirectional-scattering-distribution-functions [69,84]. Light transmission and reflection between the external and internal environment are solved with individual matrixes within the five-phase method. Compared to previous approaches in the three-phase method [80,85], an advantage is the subdivision of the sky illuminance into the direct solar and diffuse sky components, making the overall daylighting simulation results more accurate and realistic in appearance. In Equation (2), the relationship between the different matrices within the five-phase method is expressed as follows:

$$E = VTDS - V_d\, TD_d\, S_d + C_{ds}\, S_{sun} \qquad \text{Equation 2}$$

Where *E* is the illuminance matrix of the internal space, *V* is the view matrix, *T* is the transmission matrix, *D* is the daylight matrix, and S is the sky vector. Each sky vector contains an average sky luminance value of a discretized sky patch for the specific sky luminance pattern of a point-in-time conforming together the sky matrix in a dome of 145 patches [86,87]. The direct sun components of the view matrix, daylight matrix and

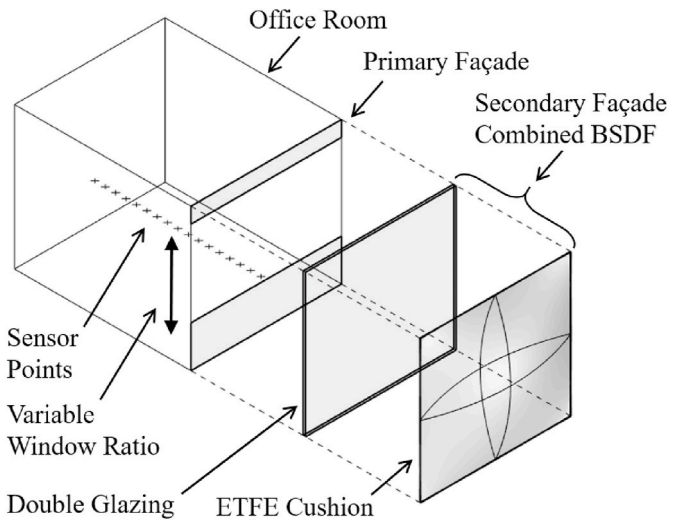

Fig. 17. Schematic room model for daylight simulation.

sky vector in Equation (2) are then replaced by the sun matrix S_{sun} and the daylight coefficient matrix C_{dc} for direct sun, resulting in an enhanced representation of direct and diffused daylight. A diagram in Fig. 16 shows the individual matrix transitions in a simplified daylight simulation scene:

2.6.2. Office geometry, simulation scenarios and parameters

The office model adopted for this simulation study is based on the minimum standard size for a single unit office according to DIN EN 4543–1:1994–09 [88] measuring 3.4 × 2.9 × 2.75 m (L-W-H). The model was generated using parametric control functions of Honeybee/Grasshopper in the 3D environment of Rhinoceros [89]. The southward-oriented wall represented the outer-façade while all other space dividing elements would have adjoining spaces. Since the five-phase method includes only three flux phases and the use of non-coplanar elements is limited [90], the DSF glazing and ETFE had to be combined into one single proxy geometry for the BSDF, covering the whole façade area. The window-to-wall ratio was adjusted separately with two variable wall elements on the interior side of the DSF façade, as shown in Fig. 17. An overview of the window-to-wall ratio scenarios is shown in Fig. 18 A-E, representing a simplified front view of the office room façade.

Additionally, five scenarios with different material combinations were defined. The first scenario is the reference scenario of clear double glazing: the other four comprised double glazing and an ETFE cushion as the second layer of the DSF. For scenario number two, a clear ETFE double-layer cushion was added to the DG. Scenario three includes a double layer ETFE cushion with a silver fritted outer layer. Scenarios four and five consisted of switchable triple-layer ETFE cushions, with scenario four representing the existing mock-up and scenario five an improved theoretical model with optimized reflectance and transmittance characteristics.

An overview of the DSF material scenarios is listed in Table 4.

All other walls, ceiling and floor elements were modelled using a grey (RGB = 186/186/186) opaque plastic material from the Radiance library, with a diffuse reflectance of 35% and a specularity and material roughness of zero. The simplification of the internal environment was intended to limit internal reflections and account in the daylight analysis primarily for the transmitted light from the DSF, allowing an objective comparison between the different DSFs. For the same reason, no artificial lighting was applied to the model to simulate only the natural daylight effect independent from other factors.

The overall setup of the simulation parameters was informed by the literature and previous daylight studies using Radiance [63,86,91,92]. An overview of the main Radiance input parameters chosen for the daylighting simulation procedure is shown in Table 5.

The sensor grid distributions for the illuminance simulation were defined in close accordance with the international Standard 12464–1:2011 (Part 1), for the lighting of indoor workplaces [93]. For the useful daylight illuminance (UDI), a total of 221 vertical sensors arranged in a regular grid of 0.2 × 0.2 m at 0.75 m height on a horizontal plane were required. For the simplified daylight glare probability (DGPs), one single vertical sensor was placed at a distance of 1.7 m facing the east wall of the room at the height of 1.2 m, representing a typical side-lit working situation. The daylight illuminance uniformity ratio (UR) was assessed with a regular 0.1 m × 0.1 m grid of 128 sensors distributed regularly over an area of 0.8 × 1.6 m at the height of 0.75 m, representing an office desk surface. Plan views of the room depicting the sensor grids are shown in Fig. 19 A-C.

2.6.3. Weather data

In order to understand ETFE DSF daylighting performance under different climate conditions, three cities in three different climate zones were selected: London, Barcelona and Shanghai. These cities are located at 51.5°, 41.4°, 31.2° N, respectively, covering 20° of latitude within the temperate and subtropical zones of the northern hemisphere. All three cities are at sea level and exposed to a maritime climate influence. However, solar irradiation and the available amount of light in each city varies significantly throughout the seasons, according to the characteristics of the corresponding Köppen-Geiger climate classification:

London (Oceanic-*Cfb*) receives an average of 1460 h of sunlight per year with an average of 3:59 of sunlight per day, and it is sunny 33.3% of

Table 4
Material combinations for double-skin façades.

Index	Material combination for double-skin façades
1	Clear Double Glazing
2	Clear Double Glazing + clear ETFE double-layer foil cushion
3	Clear Double Glazing + fritted ETFE double-layer foil cushion
4	Clear Double Glazing + printed ETFE triple-layer foil cushion, switchable
5	Clear Double Glazing + printed ETFE triple-layer foil cushion, switchable (modified)

Table 5
Simulation Parameters for Radiance daylighting simulation.

Ambient Bounces (-ab)	Ambient Divisions (-ad)	Ambient Supersamples (-as)	Ambient Resolution (-ar)	Ambient Accuracy (-aa)
10	2048	2048	64	0.200

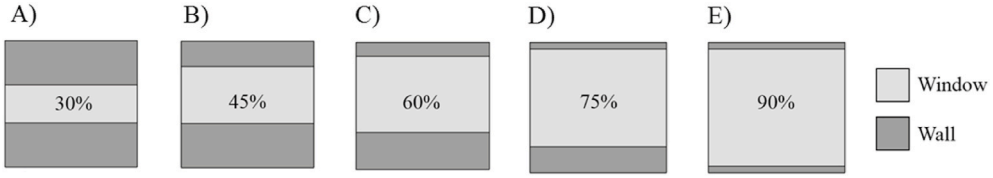

Fig. 18. Window-to-wall ratio scenarios for daylighting simulation.

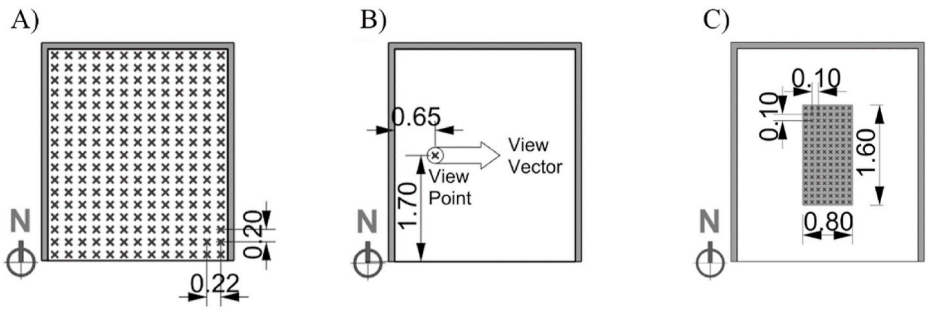

Fig. 19. Plan views of the office room showing the sensor grid distribution for UDI (A), DGPs (B), and UR (C).

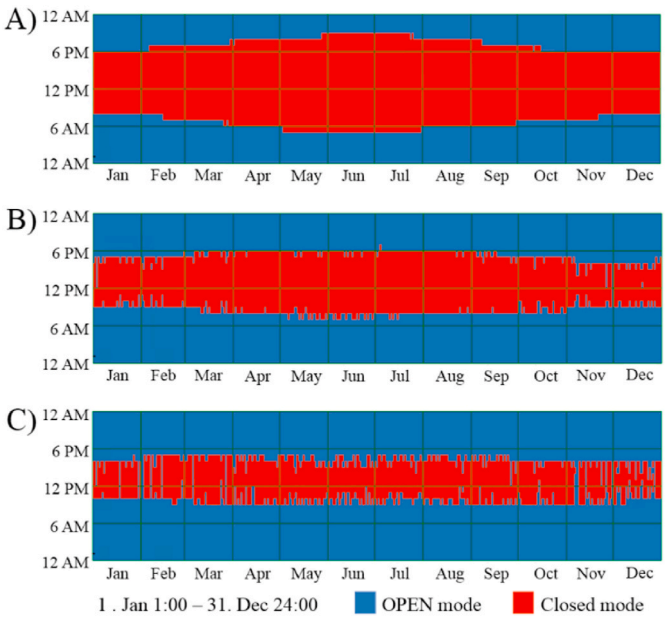

Fig. 20. Annual, hourly switching schedule for Barcelona climate with different luminance sensor thresholds: A) 0lx (closed mode = 100% sun-hours), B) 500lx (closed mode = 68% sun-hours), C) 1000lx (closed mode = 45% sun-hours).

the daylight hours with an overcast sky during the remaining 66.7% of the hours. In contrast, Barcelona (Mediterranean-*Csa*) has an average of 2437 sunlight hours per year with an average of 6:40 h per day, of which 55.6% of daylight hours are sunny. Shanghai (Sub-Tropical-*Cfa*) counts on average 1874 h of sunlight per year with an average of 5:07 h of sunlight per day, and it is sunny for 42.8% of the daylight hours and cloudy during the remaining time.

For the daylight simulation, annual weather files in EnergyPlus Weather Format (EPW) with hourly climate data based on IWEC meteorological data were used. The Figures in Appendix A display a data outtake with annual graphs for each city's direct and diffuse solar radiation patterns on a monthly basis. Data indicates that London is exposed to a total annual solar global horizontal irradiation (GHI) of 1023 kWh/m^2, Barcelona to 1621 kWh/m^2 and Shanghai to 1325 kWh/m^2. While average monthly weather data provides a good overview of each city's annual solar radiation patterns, it lacks information on specific days and hours where shading might be required. The graphs in Appendix B offer a more detailed view of the solar radiation patterns and potential critical peaks, showing the hourly global horizontal radiation in Wh/m^2. All three cities receive the highest solar radiation values in the summer months between April and September in the hours between 10am and 2pm. While not a surprising fact, it further justifies investigating adaptive building envelopes to mitigate the peaks of solar radiation responding actively to climate conditions.

2.6.4. Switch control strategy

Another important aspect for the realistic performance prediction of switchable ETFE is the calibration of the control mechanism. The luminance threshold of the control sensors determines when the ETFE will switch from one state to the other. Setting the luminance threshold at the right level is crucial for achieving the best daylight conditions within the space.

To outperform a conventional static façade system, the switching threshold needs to be set at a convergent point to achieve maximum hours of quality daylighting and minimal disturbance due to glare and inconvenient daylight distribution. If the threshold is too high, the shading mechanism might switch to closed mode, only when glare is

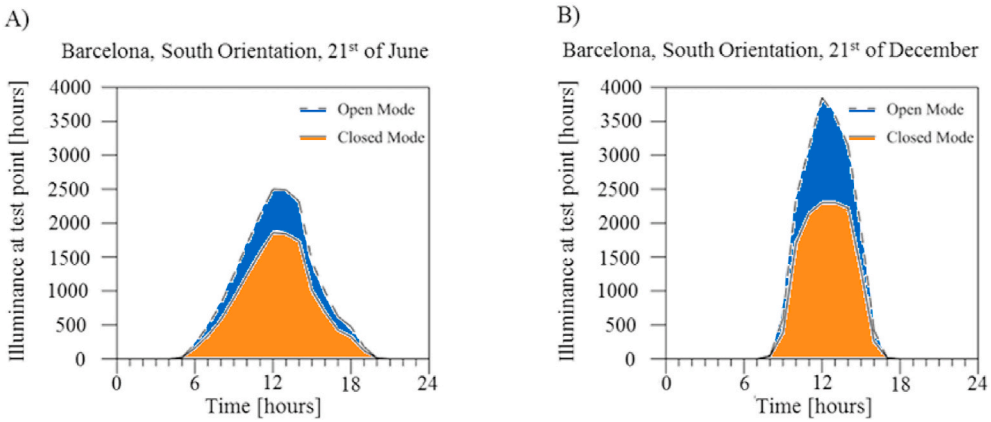

Fig. 21. Hourly Illuminance values for the summer solstice A) and winter solstice B) in open and closed mode, simulated under Barcelona climate conditions, recorded at a centred sensor point with a switch threshold of 1000lx.

already unbearable, and switch back to open mode when daylight is still beyond comfort conditions. On the other hand, when the threshold is set too low, the adaptive mechanism might stay in closed mode during most working hours when natural daylight is needed. After a preliminary analysis with all three climate files, a threshold of 1000lx was adopted with the corresponding switching schedule shown in Fig. 20 C. This setting limits the switching of the cushion to the peak hours of solar incidence, maximizing daylight and minimizing glare. The graphs in Fig. 20 A and B, in contrast, show switching schedules for lower threshold settings with the switchable ETFE in the open for fewer hours of the year.

Equally important for the performance of the switchable ETFE is the position and orientation of the virtual luminance sensor. For the threshold calibration, the sensor was positioned horizontally at 0.75 m height within the principal task area in the centre of the room model. Fig. 21 shows two graphs with the illuminance recorded at a test point at the centre of the space simulated over 24 h, with a Barcelona climate file, demonstrating the performance of the switchable ETFE with a 1000lx threshold.

Graph A in Fig. 21 shows the illuminance plotted for both switching modes on the 21st of June, the summer solstice and graph B for the winter solstice, the 21st of December. For both test periods the illuminance can be reduced and kept within the 2000lx range when switched in peak hours to the closed mode and during morning and evening hours to open mode. At the summer solstice an amplifying effect on useful daylight hours is clearly notable, whereas at the winter solstice a reducing effect on daylight intensity is more predominant. This can be explained with the extended hours of solar daylight exposure during the summer period, and the effective control of direct incidence at lower solar angles on the south façade in wintertime.

2.6.5. Dynamic daylight metrics

The metrics used in this study to evaluate the daylighting performance are dynamic, intending to provide a comprehensive annual overview rather than focussing on a specific point in time situations. Hourly results are summarized according to the established daylighting metrics of useful daylight illuminance (UDI), glare probability (DGPs) and illuminance uniformity (UR). The theoretical background and methodological approach of these metrics are outlined in the following three sections.

2.6.5.1. Useful daylight illuminance metrics. Useful daylight illuminance is a common metric used in daylighting studies to evaluate dynamic daylighting performance of architectural spaces [47,94–100]. Therefore, UDI was considered an appropriate metric to evaluate different design options of switchable ETFE double-skin façades. The concept of UDI informs how often in the year daylight illuminance is achieved within a range that is useful for a specific task or user profile. The UDI is expressed in percentage of time, providing a comprehensive numerical value that can represent the time and space dimension simultaneously [101]. Useful daylight illuminance usually falls within 100–2000lx. However, the range was adjusted for this study to fit the purpose of evaluating the daylighting conditions of office spaces. International building standards recommend illuminance levels of a minimum of 500lx for an office, where typically tasks like writing, typing, reading and data processing are carried out [93,102]. Consequently, all values below 500lx were considered as undersupply, requiring additional artificial lighting, and illuminance values above 2000lx were defined as excessive oversupply, which might cause glare.

2.6.5.2. Daylight glare probability metrics. Work in office spaces can be affected negatively by glare caused by incoming bright, unfiltered sunlight through windows. Direct or reflected creates visual discomfort, which affects the capacity to focus on a specific task, manually or intellectually. Glare creates adverse visual conditions with excessive light contrast, making it difficult to distinguish details and objects [103]. Methods to estimate the probability of glare in architectural spaces have been discussed extensively in the literature [82,104–112,113,90,73,114,115,99,116,117,118]. The method used in this study is based on the simplified daylight glare probability (DGPs) developed by Wienold, defined in the following equation:

$$DGPs = 6.22 \times 10E\text{-}5 \times E_v + 0.184 \quad \text{Equation 3}$$

where E_v is the vertical illuminance in lux at eye-level height, multiplied and summed with correction factors.

In this study, hourly Illuminance values were captured for an entire year with a vertical sensor within the simulation scene of the office space. Glare probability was evaluated according to four established categories with less than 0.35 corresponding to 'imperceptible', 0.35–0.4 to 'perceptible', 0.4–0.45 to 'disturbing' and 0.45 and above, counting as 'intolerable'.

2.6.5.3. Daylight illuminance uniformity metrics. Daylight uniformity is of importance for a task to be carried out in a specific working area and may lead to higher productivity, a better work quality, and a higher level of safety [93]. However, achieving well-distributed natural lighting on a specific task area is often challenging due to the changing environmental conditions and decreasing daylight availability along the section of the room. The daylight illuminance uniformity ratio (UR) is a metric to quantify the homogeneity of light availability over a specific area. UR is based on horizontal illuminance values and provides a percentage of evaluated hours with the available daylight uniformity bins, of $\leq$0.4, 0.4–0.6, 0.6–0.7 and $\geq$ 0.7 for an evaluated task area [99,119]. BS EN 12464–1:2011 requires office spaces to achieve an UR of 0.4–0.6 in the task area and in the immediate surrounding area $\geq$0,40 while the background area shall be $\geq$ 0,10. For the simulation scenario, a hypothetical task area with dimensions of a generic office desk was positioned at the centre of the virtual office room.

3. Results and discussion

The following sub-sections display the results obtained from the annual daylighting simulation for one single unit office space. Hourly results for a typical office schedule (9am-5pm, Mon.-Fri.) were summarized according to the established daylighting metrics of useful daylight illuminance (UDI), glare probability (DGPs) and illuminance uniformity (UR). The daylighting conditions for different performance criteria are discussed independently and then compared for a multi-objective ranking of the applicability of the different DSF materials.

3.1. Useful daylight illuminance results

The results for the UDI are based on annual illuminance simulations that provide a comprehensive overview of the daylighting illuminance of the office space with DSF designs under different climate conditions. The general trend observed in all analysed scenarios is that the UDI in the office with the double glazed and clear ETFE DSF increases gradually across the room's section towards the back of the room. This can be explained by the total illuminance levels close to the window, which are much higher than the established UDI range, dropping sharply after a 1-m distance and levelling down towards the back of the room where UDI is achieved. For the cases with fritted and switchable ETFE double-skin façade, the incident solar radiation is reflected in large parts by the outer layer of the ETFE cushions. As a result, the internal illuminance levels are reduced and do not contrast as severely across the room section as in the case with double glazing only. Therefore, the overall percentage of time with UDI is higher with fritted and switchable ETFE than double-glazing and clear ETFE. The higher UDI values for these two DSF types are concentrated, spatially, in the centre of the room. In contrast, the highest UDI values for the double glazing and clear ETFE were

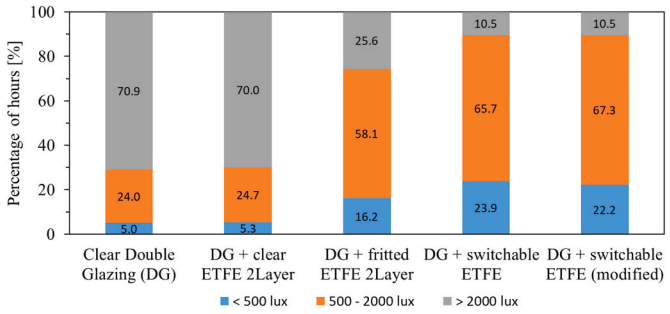

Fig. 22. Annual UDI, Shanghai, 90% WWR

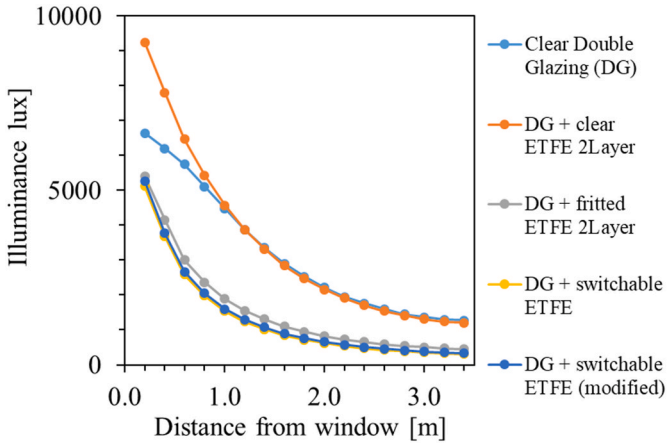

Fig. 23. Shanghai, 21st of June, 12.00 a.m.

shifted towards the back of the room. This observation strengthens the hypothesis that double-skin façades with fritted or switchable ETFE deliver a better daylighting performance than a single façade with double-glazing. A double-skin façade with clear ETFE might also not contribute to significant improvements. The graphs in Figs. 22 and 23 support the above observations, comparing the annual UDI of Shanghai with the point in time illuminance across the centre section of the room, starting from the south-facing window towards the north-facing internal wall with a WWR of 90%.

In Fig. 24, the UDI performance trends were plotted for a selected test point at the centre of the room across all analysed WWR scenarios. While this type of analysis does not represent the performance of the whole room, it provides an objective comparison of the effect that the parameters of climate, WWR and façade material have on the percentage of annual UDI. The general trend observed from the graphs is that, independently of the climate scenario, the annual hourly percentage of UDI in the office space decreases with augmenting WWRs when double-glazing single-skin or clear ETFE double-skin façades are employed. The opposite performance trend is observed for the DSF with the fritted and switchable ETFE cushion, showing a higher annual hourly percentage of UDI for increasing WWR. This leads to the interpretation that for large window façades, it would be better to use fritted or switchable ETFE as a measure for retrofitting, while for façades with small window sizes, the most suitable solution for retrofit would be, depending on the location, a DSF with clear ETFE or double glazing only. These results appear reasonable when compared with recent studies on conventional internal window shades [120,121]. The horizontal UDI plots in Figs. 25–27, for London, Barcelona and Shanghai, respectively, reinforce this interpretation but deliver a bigger picture of the overall performance. The UDI plots, in plan view, show the annual UDI for every single point of the test grid and provide an overview of the UDI levels for the whole room at desk height. What becomes evident is that the switchable ETFE cushion provides a daylight exposure focussed in the centre area of the room, while for the scenario with the fritted ETFE, the best-illuminated area is shifted from the centre towards the interior end of the room. In a room with a sizeable window-to-wall ratio, a widespread illuminated area in the centre of the room is more likely to be achieved with a switchable ETFE cushion, while for a small WWR, this effect is more effectively achieved with a fritted ETFE cushion. The only scenario where the double-glazing without any additional façade skin was observed to be more beneficial in terms of useful daylight illuminance was the room with the smallest window-to-wall ratio. At 30% WWR, double glazing provided more useful daylighting hours on a wider room area than any other investigated façade design, a pattern that was observed in all three climate scenarios. Overall, the results show that switchable ETFE DSFs provides equally satisfying, if not better natural lighting conditions in office spaces when applied as a retrofitting measure to the building envelope.

3.2. Daylight glare probability results

The results for the daylight glare probability obtained for the different climate scenarios and DSF material combinations are summarized in Tables 6–8. The tables show the percentage of time when glare is either intolerable, disturbing, perceptible, or imperceptible during the assumed occupied office hours. The results obtained for London, listed in Table 6, show that the glare probability within the office increases with

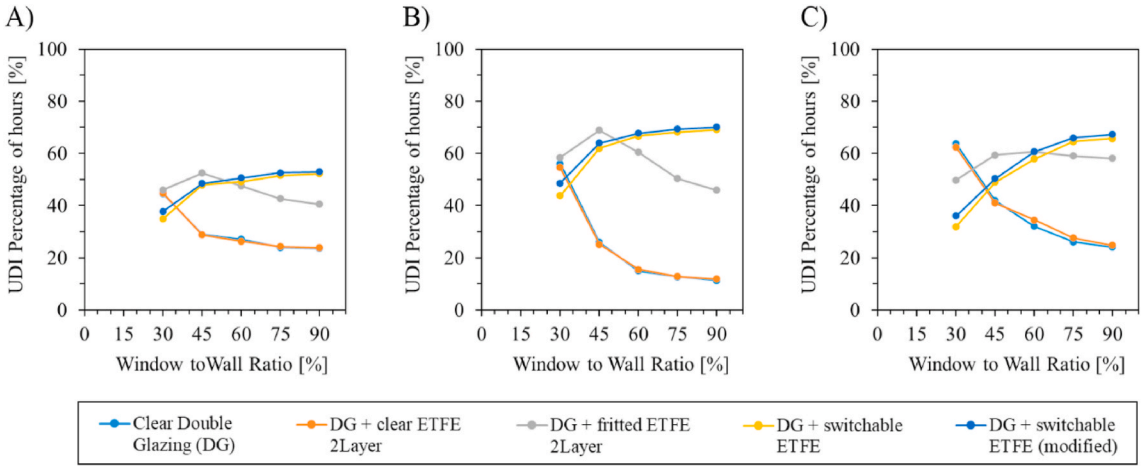

Fig. 24. Annual UDI, 500–2000lx bin at the centre of the room for different double-skin façades with varying WWRs across different climates: A) London, B) Barcelona, C) Shanghai.

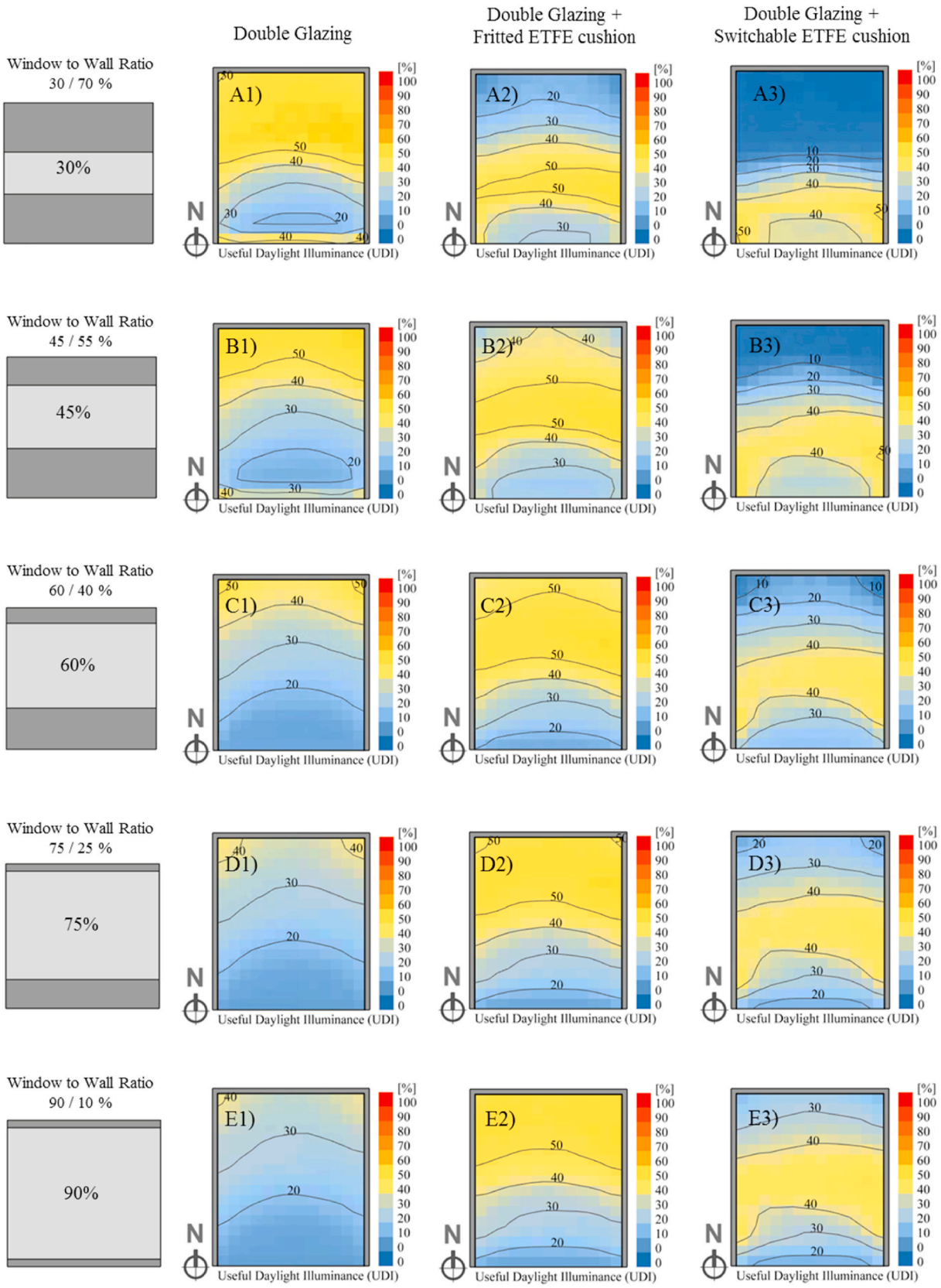

Fig. 25. Annual UDI, 500–2000lx bin at 0.75 m height horizontal plan for a 5-day working hours schedule of a south-facing office in London: DG (1), DG + fritted ETFE cushion (2) and DG + switchable ETFE cushion (3), for different WWR ratios: A) 30%, B) 45%, C) 60%, D) 75%, E) 90%.

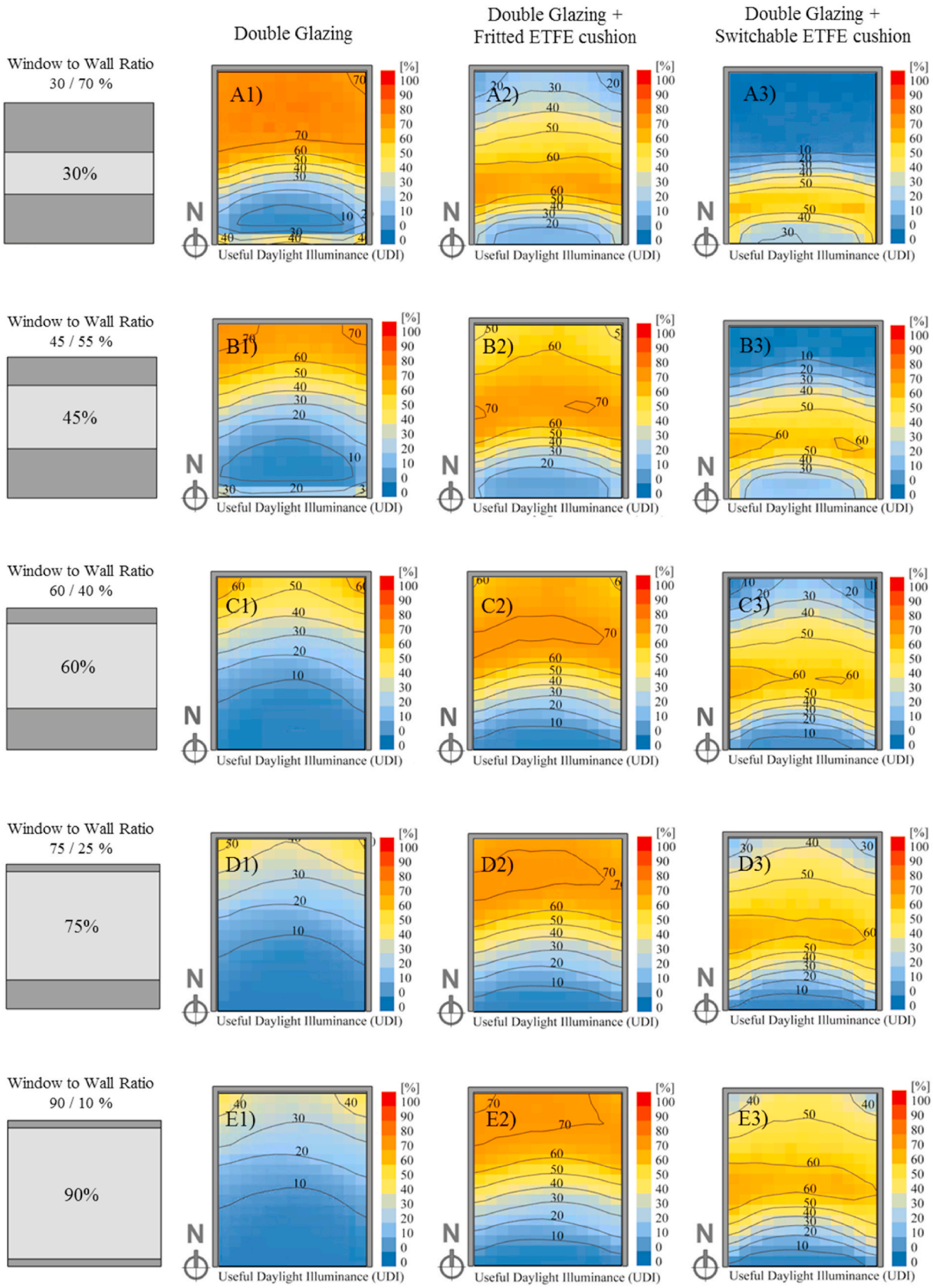

Fig. 26. Annual UDI, 500–2000lx bin at 0.75 m height horizontal plan for a 5-day working hours schedule of a south-facing office in Barcelona: DG (1), DG + fritted ETFE cushion (2) and DG + switchable ETFE cushion (3), for different WWR ratios: A) 30%, B) 45%, C) 60%, D) 75%, E) 90%.

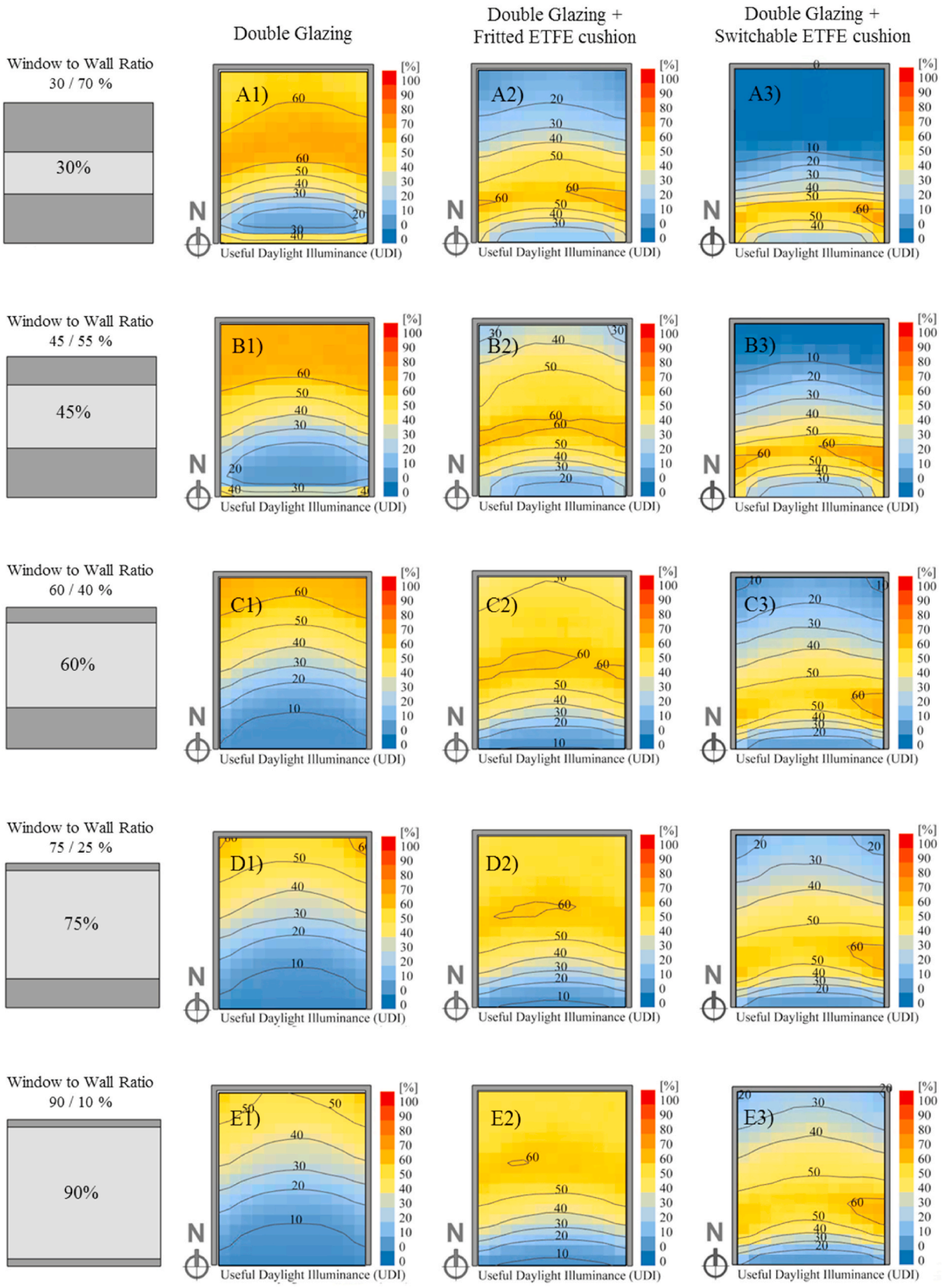

Fig. 27. Annual UDI, 500–2000lx bin at 0.75 m height horizontal plan for a 5-day working hours schedule of a south-facing office in Shanghai: DG (1), DG + fritted ETFE cushion (2) and DG + switchable ETFE cushion (3), for different WWR ratios: A) 30%, B) 45%, C) 60%, D) 75%, E) 90%.

Table 6
Simplified Daylight Glare Probability (DGPs): numerical data summary for London.

WWR	Glare Perception	Bin	Clear Double Glazing (DG)	DG + clear ETFE 2 Layer	DG + fritted ETFE 2 Layer	DG + switch. ETFE 3 Layer	DG + switch. ETFE modif.
30%	Imperceptible:	≤0.35	92.16%	93.21%	98.87%	97.17%	97.17%
	Perceptible:	0.35–0.4	5.13%	4.44%	0.44%	0.44%	0.44%
	Disturbing:	0.4–0.45	0.36%	0.24%	0.12%	0.16%	0.16%
	Intolerable:	≥0.45	2.34%	2.10%	0.57%	2.22%	2.22%
45%	Imperceptible:	≤0.35	70.06%	68.20%	96.77%	94.51%	94.46%
	Perceptible:	0.35–0.4	16.04%	17.74%	0.53%	0.48%	0.48%
	Disturbing:	0.4–0.45	6.91%	8.24%	0.61%	0.40%	0.44%
	Intolerable:	≥0.45	6.99%	5.82%	2.10%	4.61%	4.61%
60%	Imperceptible:	≤0.35	56.61%	55.68%	95.31%	93.25%	93.13%
	Perceptible:	0.35–0.4	15.84%	14.87%	1.01%	0.53%	0.65%
	Disturbing:	0.4–0.45	12.73%	13.41%	0.69%	0.44%	0.40%
	Intolerable:	≥0.45	14.83%	16.04%	2.99%	5.78%	5.82%
75%	Imperceptible:	≤0.35	49.66%	49.66%	94.67%	92.61%	92.40%
	Perceptible:	0.35–0.4	11.56%	10.30%	1.33%	0.85%	1.05%
	Disturbing:	0.4–0.45	14.79%	13.86%	0.57%	0.57%	0.57%
	Intolerable:	≥0.45	24.00%	26.18%	3.43%	5.98%	5.98%
90%	Imperceptible:	≤0.35	47.60%	46.91%	89.29%	92.32%	92.24%
	Perceptible:	0.35–0.4	10.14%	9.25%	6.51%	1.13%	1.21%
	Disturbing:	0.4–0.45	12.73%	11.64%	0.65%	0.57%	0.44%
	Intolerable:	≥0.45	29.54%	32.20%	3.56%	5.98%	6.10%

Table 7
Simplified Daylight Glare Probability (DGPs): numerical data summary for Barcelona.

WWR	Glare Perception	Bin	Clear Double Glazing (DG)	DG + clear ETFE 2 Layer	DG + fritted ETFE 2 Layer	DG + switch. ETFE 3 Layer	DG + switch. ETFE modif.
30%	Imperceptible:	≤0.35	89.05%	89.33%	98.83%	98.22%	98.22%
	Perceptible:	0.35–0.4	9.21%	9.09%	0.36%	0.04%	0.04%
	Disturbing:	0.4–0.45	0.20%	0.20%	0.28%	0.20%	0.20%
	Intolerable:	≥0.45	1.54%	1.37%	0.53%	1.54%	1.54%
45%	Imperceptible:	≤0.35	60.77%	58.38%	93.82%	92.12%	92.12%
	Perceptible:	0.35–0.4	16.08%	18.91%	0.73%	0.24%	0.24%
	Disturbing:	0.4–0.45	10.63%	13.49%	1.09%	0.36%	0.36%
	Intolerable:	≥0.45	12.53%	9.21%	4.36%	7.27%	7.27%
60%	Imperceptible:	≤0.35	42.22%	37.98%	91.35%	89.66%	89.66%
	Perceptible:	0.35–0.4	21.17%	20.89%	0.85%	0.48%	0.44%
	Disturbing:	0.4–0.45	11.80%	14.99%	1.45%	0.36%	0.36%
	Intolerable:	≥0.45	24.81%	26.14%	6.34%	9.49%	9.54%
75%	Imperceptible:	≤0.35	33.70%	31.43%	89.37%	88.36%	88.36%
	Perceptible:	0.35–0.4	15.56%	13.98%	1.82%	0.61%	0.48%
	Disturbing:	0.4–0.45	16.57%	17.98%	1.17%	0.61%	0.69%
	Intolerable:	≥0.45	34.18%	36.61%	7.64%	10.42%	10.46%
90%	Imperceptible:	≤0.35	29.01%	27.84%	83.31%	88.32%	88.28%
	Perceptible:	0.35–0.4	13.25%	10.55%	7.64%	0.40%	0.40%
	Disturbing:	0.4–0.45	17.41%	14.59%	0.81%	0.77%	0.77%
	Intolerable:	≥0.45	40.32%	47.03%	8.24%	10.51%	10.55%

larger WWR for façades with simple double-glazing and DG with added clear ETFE. With a 30% WWR, the glare is imperceptible for 92% and 93% of the office hours for DG and DG + clear ETFE, respectively. For a WWR of 90%, glare is perceptible 10% of office hours, 12% of the time disturbing and intolerable for 32% of the working hours: hence, the visual working environment is unacceptable for up 44% of the time, due to glare. The immediate conclusion from the results is that DG and clear ETFE DSF are not suitable to control glare in south-facing office façades in London, especially when the WWR is large. However, the results from the other DSF material combinations, with fritted and switchable ETFE, show a reduced glare probability for all WWR scenarios and prove the effectiveness of this retrofitting measure. Independent of window sizes, the glare inside the room is imperceptible during 92–97% of the office working hours when fritted or switchable ETFE is applied. In climates with intense solar radiation and more daylight availability throughout the year, the described trend is similar.

In Barcelona (Table 7), glare is imperceptible for most working hours when using printed or switchable ETFE. For the largest WWR of 90%, the glare is intolerable for only 10% of the working hours and reduces considerably to 0.6% towards the smallest WWR with a 30% window area. For the DG and the clear ETFE façade, the percentage of working hours with intolerable glare is considerably higher, with up to 47% for the largest WWR.

In Shanghai (Table 8), a similar trend is observed for all simulated scenarios suggesting a consistent optical behaviour of the simulated façade design across different scenarios. In general, the findings indicate that fritted or switchable ETFE façades could reduce the probability of glare for a range of climates when employed as a second layer in a DSF. The reflective properties of the frit prints in combination with the light scattering behaviour of the material and shape of the ETFE cushion are suggested as the reason for the effective control of glare.

The switching capabilities of the adaptive façade were expected to reduce the glare even better during the peak hour of direct incident solar radiation; however, the results show that this was only true for the largest WWR (90%), and static frit prints were as effective. The density and smaller scale of the print pattern may have been a related factor, by scattering light more effectively over a large surface than a larger pattern with clear ETFE sections, as is the case for the switchable ETFE, thus leading to reduced glare. This finding is important for developing new printing patterns for ETFE cushions to be applied specifically in

Table 8
Simplified Daylight Glare Probability (DGPs): numerical data summary for Shanghai.

WWR	Glare Perception	Bin	Clear Double Glazing (DG)	DG + clear ETFE 2 Layer	DG + fritted ETFE 2 Layer	DG + switch. ETFE 3 Layer	DG + switch. ETFE modif.
30%	Imperceptible:	≤0.35	91.68%	92.65%	100.00%	100.00%	100.00%
	Perceptible:	0.35–0.4	8.32%	7.35%	0.00%	0.00%	0.00%
	Disturbing:	0.4–0.45	0.00%	0.00%	0.00%	0.00%	0.00%
	Intolerable:	≥0.45	0.00%	0.00%	0.00%	0.00%	0.00%
45%	Imperceptible:	≤0.35	76.65%	75.64%	98.59%	98.42%	98.42%
	Perceptible:	0.35–0.4	8.20%	8.85%	0.00%	0.00%	0.00%
	Disturbing:	0.4–0.45	7.88%	12.24%	0.04%	0.04%	0.04%
	Intolerable:	≥0.45	7.27%	3.27%	1.37%	1.54%	1.54%
60%	Imperceptible:	≤0.35	64.77%	61.94%	95.72%	95.60%	95.60%
	Perceptible:	0.35–0.4	12.85%	14.38%	0.36%	0.04%	0.00%
	Disturbing:	0.4–0.45	6.42%	6.67%	0.04%	0.04%	0.08%
	Intolerable:	≥0.45	15.96%	17.01%	3.88%	4.32%	4.32%
75%	Imperceptible:	≤0.35	54.26%	51.96%	92.97%	93.86%	93.82%
	Perceptible:	0.35–0.4	17.25%	17.01%	1.45%	0.16%	0.16%
	Disturbing:	0.4–0.45	7.72%	9.09%	0.28%	0.08%	0.12%
	Intolerable:	≥0.45	20.77%	21.94%	5.29%	5.90%	5.90%
90%	Imperceptible:	≤0.35	48.81%	47.27%	87.47%	93.74%	93.70%
	Perceptible:	0.35–0.4	16.20%	13.86%	6.91%	0.24%	0.24%
	Disturbing:	0.4–0.45	11.47%	13.33%	0.24%	0.12%	0.16%
	Intolerable:	≥0.45	23.52%	25.54%	5.37%	5.90%	5.90%

building façades as a retrofitting measure or for new builds.

3.3. Daylight illuminance uniformity results

This section discusses the simulation results for daylight uniformity. Overall, the graphs A to E in Fig. 28 suggest that the DSF design with the fritted ETFE provides the highest percentage of working hours with a well-distributed daylight uniformity across all simulated scenarios. The double-glazing alone and the DSF with clear ETFE tend to perform better with smaller WWRs of 30%–45%, whereas the DSF with switchable ETFE delivers better performance in terms of UR in the scenarios with larger WWRs, from 60% to 90%.

For climates like Shanghai, which already receive a higher proportion of diffuse daylight during the year, comfortable internal daylight uniformity ratios are available for more office working hours than in climates with more direct solar radiation, like in Barcelona.

However, climates like London with a pronounced variability of sunlight availability across the seasons show no reduction of UR in the 0.4–0.6 range, an effect which would have initially been expected due to fewer daylight hours during the winter season. UR in the desired range (0.4–0.6) was achieved on average for approximately 60% of office hours across all scenarios, with little variability among the façade materials. The only exceptions were the scenarios with large WWR and a simple double-glazed façade, resulting in fewer hours in the desired UR range. For Barcelona, the UR was on average 50% of the hours within the targeted range across most WWR scenarios. Only with a larger WWR from 65% to 90%, the percentage of hours dropped notably around 10%–15%. A possible explanation is the intense direct solar radiation and the associated higher contrast of shade and light projected into the room, typical for Mediterranean climates like Barcelona. For Shanghai, the uniformity ratio was throughout all scenarios high, ranging between 65% and 70% on average. However, the double glazing showed a significant performance drop for large WWR with 90% aperture.

Overall, the results suggest that satisfying illuminance uniformity can be achieved in small office spaces with natural daylight. Moreover, it seems possible to achieve illuminance uniformity across different climates and latitudes. The results suggest that double-skin façades with inflated ETFE cushions as a second façade layer improve the illuminance uniformity and extend the number of working hours, with uniform daylight available up to 70% of the total scheduled working hours. Only an additional 30% of the hours would have to be supplied by artificial lighting to achieve uniform light distribution for the complete schedule. However, a high daylight uniformity value might also be interpreted as a sign of high light intensity leading to sharp contrasts in the office space beyond the working area. This situation may require more solar shading instead of additional artificial lighting. Therefore, it is not surprising that fritted ETFE cushions with improved reflective print patterns performed best among all simulated material combinations. Fritted ETFE shows a better capability to scatter and distribute diffused light evenly throughout the space than glass or clear ETFE, especially for façades with large WWR. However, only experimental settings or post-occupancy studies in real buildings might provide a definite answer to this hypothesis and confirm the findings of this simulation campaign.

3.4. Multi-objective scenario ranking

Quality daylight conditions for productive office environments require a balance of good light levels, an evenly lit work area and protection from glare. The above analysis showed that ETFE DSFs could meet the criteria individually in most simulated scenarios. However, it is of interest to understand under which conditions DSFs can provide the best performance for all criteria together. Therefore, a multi-objective analysis was carried out comparing and rating the different material options for the climate and WWR parameters. Annual values for UDI, DGPs and UR, at the center of the office room, were compiled and grouped into low- (Min ↔ $^1/_3$), medium- ($^1/_3$ ↔ $^2/_3$) and high-performance bins. An even criteria weight was assigned to all three daylight metrics (UDI, DGPs, UR), and the sum of the recorded values determined the total rating of the scenarios. Fig. 29 shows a summary chart of the multi-objective ranking.

Overall, the chart shows that the trends observed for the analysis of the individual criteria also prevail in general terms for the multi-objective analysis:

Clear ETFE provides better performance for small WWR in climates with fewer sunlight hours. In contrast, fritted and switchable ETFE is well-performing with large WWR and in climates with abundant solar light. However, only 12 out of 45 analysed scenarios (26%) meet the high-performance criteria when combining all three daylight metrics. Seven scenarios with exceptional performance were achieved with the fritted ETFE, four with switchable ETFE and one with clear ETFE. Most of these scenarios (10) were located in Shanghai, corresponding to the Sub-tropical climate conditions. Here, where solar light is available all year long, fritted and switchable ETFE performed satisfactorily for almost all WWRs, while clear ETFE only fulfilled the high-performance criteria for the smallest WWRs (30%). With fritted ETFE, the highest-ranking scenario was achieved under Sub-tropical conditions, marking

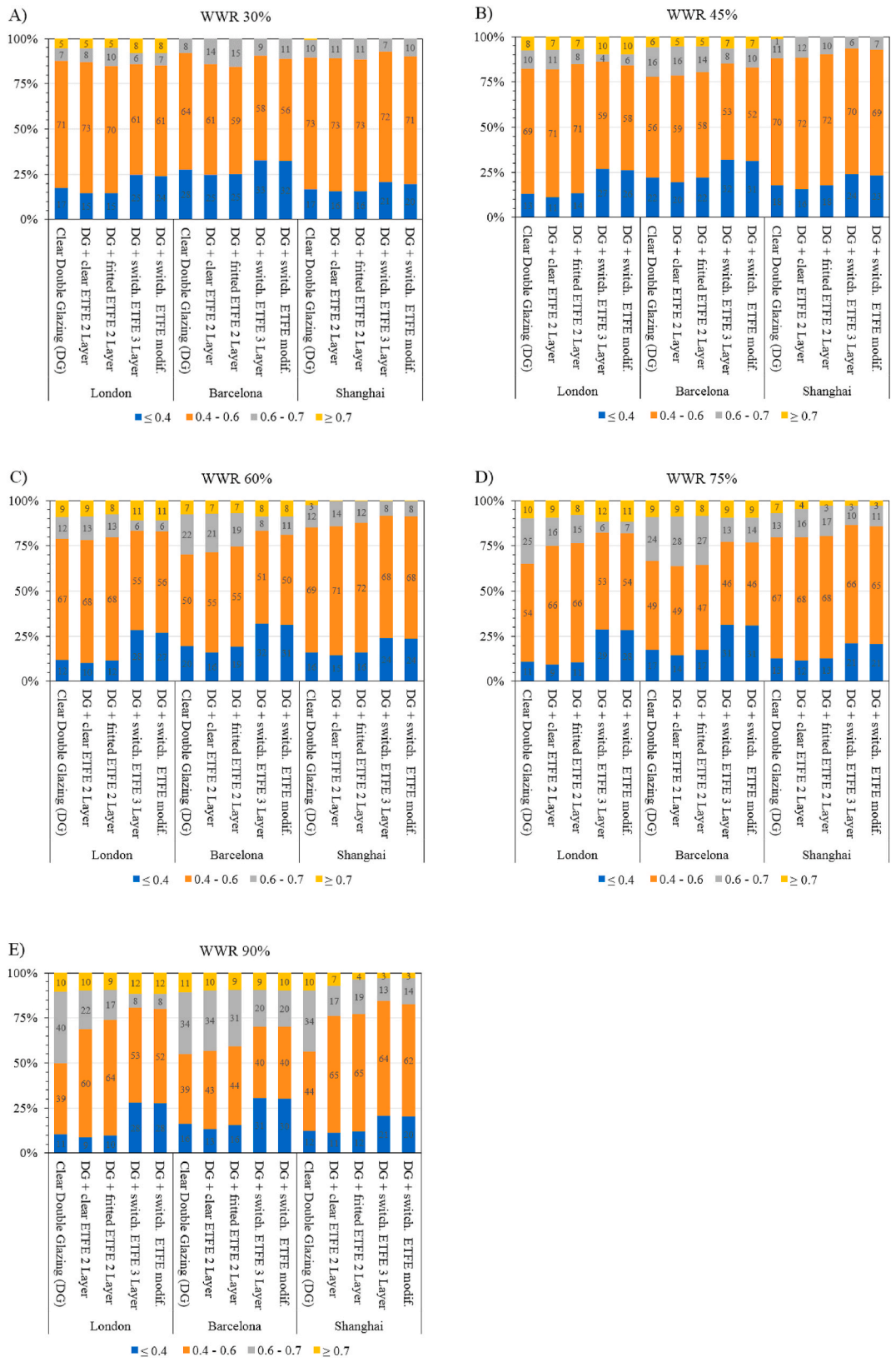

Fig. 28. Daylight illuminance uniformity ratio (UR) at task area for south-facing office under climate conditions of London, Barcelona and Shanghai with different ETFE DSF and WWRs: A) 30%, B) 45%, C) 60%, D) 75%, E) 90%.

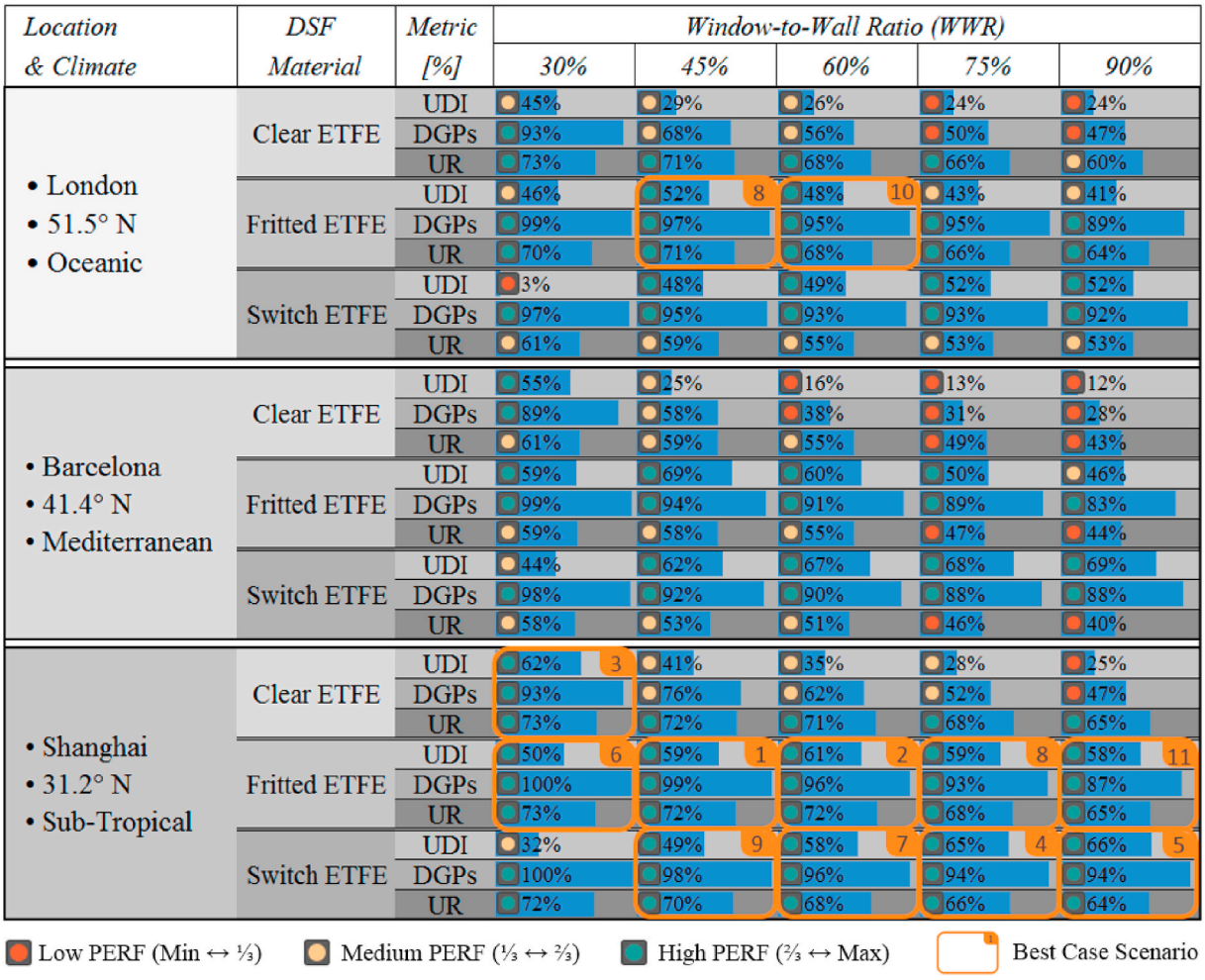

Fig. 29. Multi-objective best-case scenario ranking.

an annual UDI of 59%, DGPs of 99% and a UR of 72% for a WWR of 45%. Switchable ETFE also ranked highest in the Sub-tropical climate scenario, but for a larger WWR of 75%. The annual UDI marked 65%, DGPs 94%, and UR 66% for this scenario. The highest-ranking scenario for the DSF with clear ETFE coincided with a small WWR of 30% under Sub-tropical climate conditions, with a UDI of 62%, DGPs of 93%, and UR of 73%.

Despite the diverse scenarios where the material types performed best, the variance among the individual metrics across the three selected high-performing scenarios was relatively low, with 6.0%, 6.8% and 9.5%, for UDI, DGPs and UR, respectively. This suggests that quality daylight conditions can be achieved with all three ETFE material options for different scenarios. As a general classification of the three material options for applications in double-skin façades, fritted ETFE could be considered an "allrounder" solution that would provide satisfactory daylighting performance for a range of climates and window-to-wall ratios. Switchable ETFE would classify as a "specialized" building solution, providing good daylighting performance for complicated scenarios with medium to large WWRs in climates with abundant solar light. Clear ETFE would be considered a "fitted" material solution, reserved for small WWRs or climates with less solar light availability.

4. Conclusions

This paper investigated the daylighting performance of an office space retrofitted with different façade materials and designs. The study focussed on double-skin façades with clear, fritted and switchable ETFE and evaluated the daylighting performance with criteria of useful illuminance for office work (UDI), disturbance through glare (DGPs), and illuminance uniformity (UR). The study was carried out using ray-tracing and BSDF, performing the calculations for the daylighting simulations with the five-phase method using validated Radiance programs. The simulations were based on annual weather data and spectral analysis of ETFE materials. An array of simulation scenarios was simulated, testing the proposed double-skin façade materials under different climate conditions and a range of window-to-wall ratios. The daylight performance was evaluated using dynamic metrics based on hourly climate data, analysing and expressing UDI, DGPs and UR as a percentage of time in a spatial grid. This approach allowed to assess the overall performance of the different DSF materials in each of the scenarios. This combined methods approach, together with the creation of a physics-based optical model of switchable ETFE, is intended to be the main contribution of this paper to the daylighting performance analysis of adaptive façades.

The results obtained through this method showed that glare can effectively be reduced and better daylight uniformity achieved when employing fritted or switchable ETFE in double skin façades. Likewise, the percentage of time when useful daylight illuminance was achieved increased when using fritted and switchable ETFE cushions as a second façade. The most notable improvements of the daylighting performance with switchable ETFE DSF were in the climate scenarios with the highest annual exposure to solar radiation. Useful daylight was distributed more equally at the centre of the space when switchable ETFE cushions were employed, especially in façades with large window-to-wall ratios.

Fritted ETFE tended to improve the daylight distribution in rooms with smaller windows. In contrast, single-skin façades with double-glazing and double-skin façades with clear ETFE underperformed in almost all tested scenarios. The only exception was the climate scenario with lower solar radiation and the smallest of the analysed window-to-wall ratios; in this case, the double glazing outperformed all ETFE design options. However, even if the performance of a specific system is exceptional over the course of the year, there still will be periods of time when glare and illuminance over or undersupply will affect the qualities of daylit office spaces.

While in this study switchable ETFE cushions performed generally well as daylighting control systems in double-skin façades, a remaining task for future research is to identify key parameters for improving the energy performance. Therefore, further studies should investigate the thermal performance of ETFE DSF and the primary and secondary impacts on a building's energy consumption when employed as a retrofitting measure. Effects of façade ventilation, orientation and integration of energy-producing technologies might be other research fields worth exploring before implementing ETFE in building retrofits on a larger scale.

Declaration of competing interest

The authors declare that they have no known competing financial interests or personal relationships that could have appeared to influence the work reported in this paper.

Acknowledgements

This article is partially based on a large-scope PhD research project aimed at furthering the understanding of the environmental performance of ETFE building envelopes [122]. It was supported by the Faculty of Engineering at The University of Nottingham through a PhD studentship awarded to Jan-Frederik Flor. Additional support to this article was provided by the Engineering and Physical Sciences Research Council, UK [grant number EP/S030786/1]. The authors would also like to thank their industry partner, Architen Landrell, for generously providing all ETFE samples and manufacturing the mock-up.

Appendix A. and B. Supplementary data

Appendix A

Annual solar radiation graph showing average diffuse horizontal and direct normal radiation for London, Barcelona and Shanghai (graphs by the authors based on climate data retrieved from EnergyPlus™ [123]).

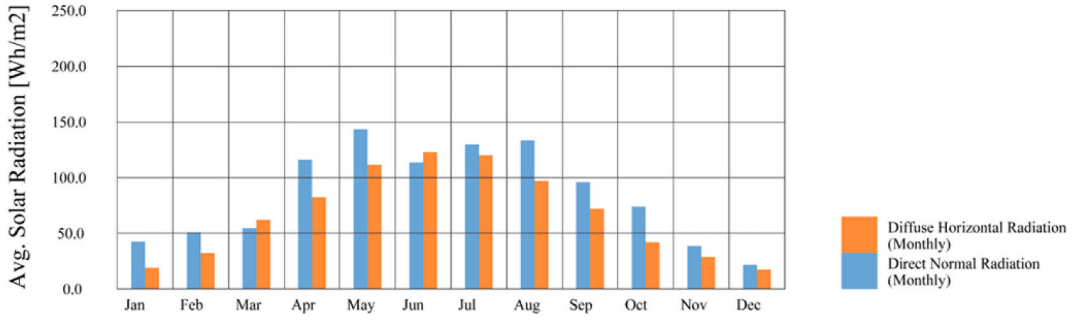

LONDON/GATWICK_GBR

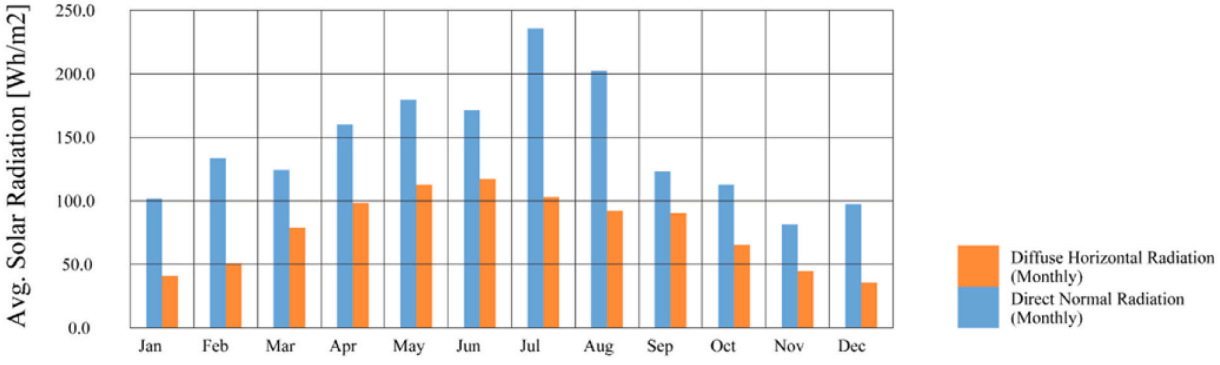

BARCELONA_ESP

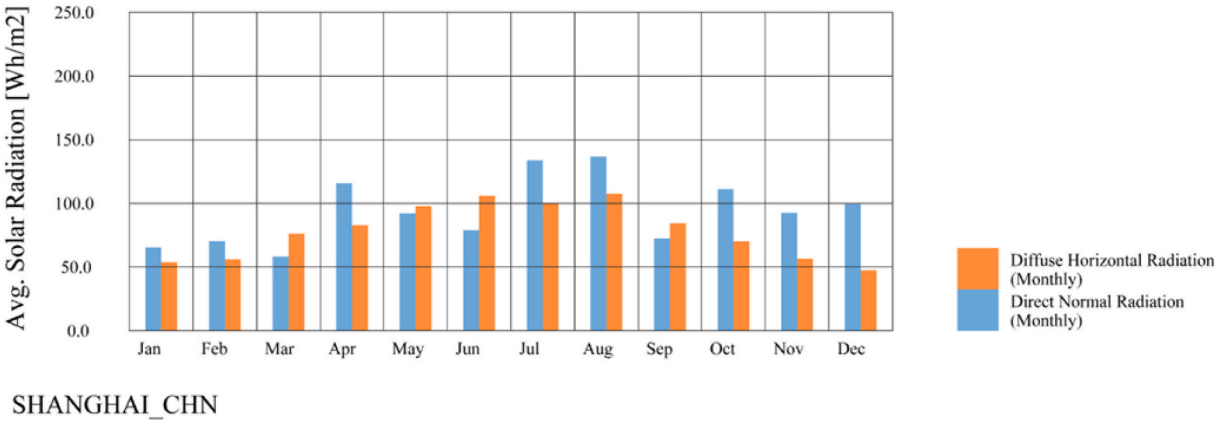

Appendix B

Annual solar radiation graphs showing the hourly global horizontal radiation for London, Barcelona and Shanghai (graphs by the authors based on climate data retrieved from EnergyPlus™ [123]).

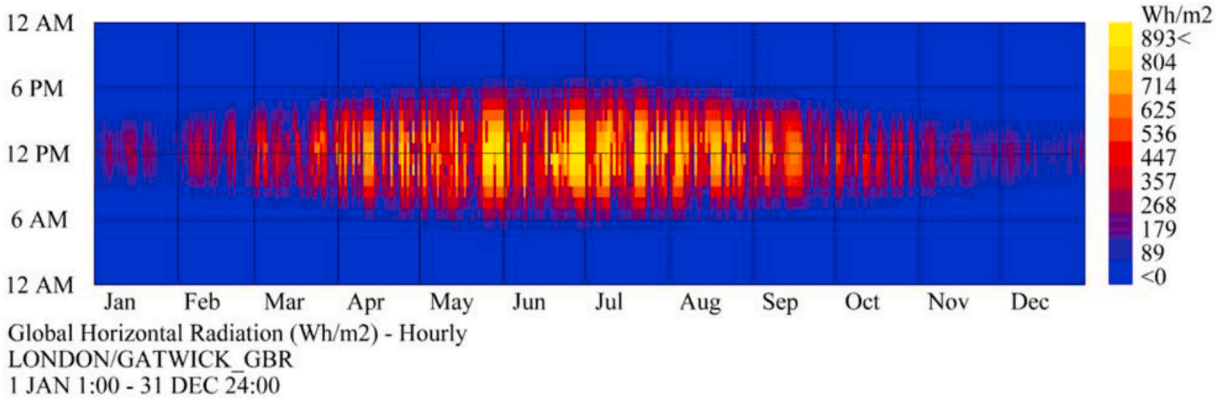

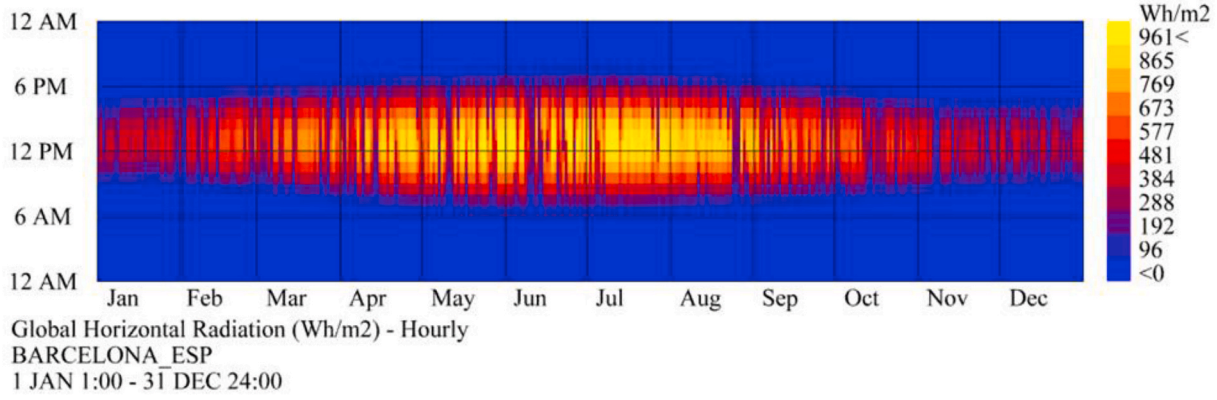

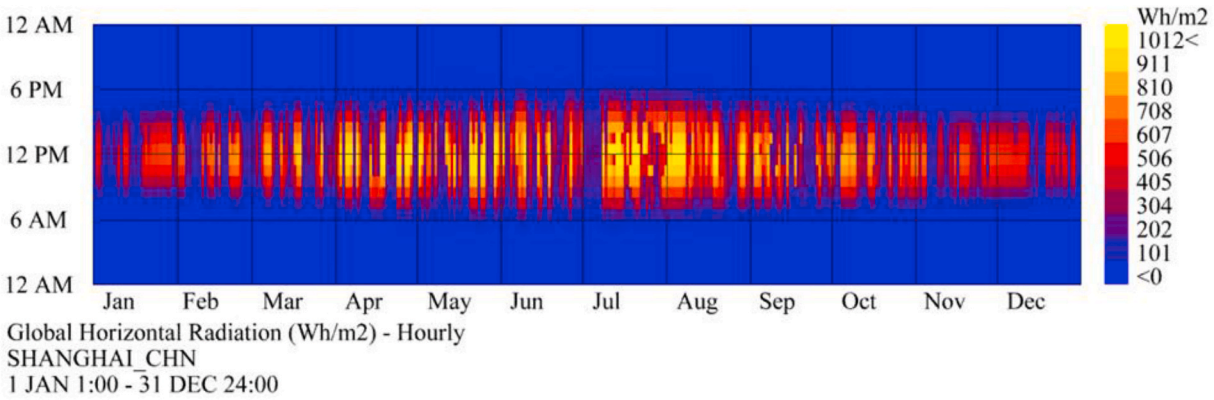

References

[1] Y. Al Horr, M. Arif, A. Kaushik, A. Mazroei, M. Katafygiotou, E. Elsarrag, Occupant productivity and office indoor environment quality: a review of the literature, Build. Environ. 105 (2016) 369–389.

[2] I. Turan, A. Chegut, D. Fink, C. Reinhart, The value of daylight in office spaces, Build. Environ. 168 (2020) 106503.

[3] A. Pellegrino, S. Cammarano, V.R.M. Lo Verso, V. Corrado, Impact of daylighting on total energy use in offices of varying architectural features in Italy: results from a parametric study, Build. Environ. 113 (2017) 151–162.

[4] M. Krarti, P.M. Erickson, T.C. Hillman, A simplified method to estimate energy savings of artificial lighting use from daylighting, Build. Environ. 40 (2005) 747–754.

[5] H. Shen, A. Tzempelikos, Daylighting and energy analysis of private offices with automated interior roller shades, Sol. Energy 86 (2012) 681–704.

[6] J. Yu, Y. Liu, C. Xiong, J.c. Huang, Study on daylighting and energy conservation design of transparent envelope for office building in hot summer and cold winter zone, Procedia Eng. 121 (2015) 1642–1649.

[7] C. Bedon, D. Honfi, M. Kozłowski, K. Machalická, F. Santos, T. Wüest, M. Eliášová, M. Vokáč, Key structural aspects for adaptive facades - activity progress from the EU-COST action TU1403 'structural' task group 2 (2018) 135–154, 6.

[8] R. Toufeili, R. Ruparathna, E. Tam, Rethinking Energy Retrofit Evaluation: A Life Cycle Thinking Based Approach, 2019.

[9] S. Seyedzadeh, F. Pour Rahimian, Multi-objective Optimisation and Building Retrofit Planning, Green Energy and Technology, 2021, pp. 31–39.

[10] Q. Li, A. Zanelli, A review on fabrication and applications of textile envelope integrated flexible photovoltaic systems, Renew. Sustain. Energy Rev. 139 (2021) 110678.

[11] G. Yun, K.C. Yoon, K.S. Kim, The influence of shading control strategies on the visual comfort and energy demand of office buildings, Energy Build. 84 (2014) 70–85.

[12] A. Michael, S. Gregoriou, S.A. Kalogirou, Environmental assessment of an integrated adaptive system for the improvement of indoor visual comfort of existing buildings, Renew. Energy 115 (2018) 620–633.

[13] F. Ascione, N. Bianco, T. Iovane, M. Mastellone, G.M. Mauro, The evolution of building energy retrofit via double-skin and responsive façades: a review, Sol. Energy 224 (2021) 703–717.

[14] J.F. Flor, Y. Sun, P. Beccarelli, C. Rowell, J. Chilton, Y. Wu, Experimental study on the thermal performance of ethylene-tetrafluoroethylene (ETFE) foil cushions, IOP Conf. Ser. Mater. Sci. Eng. 556 (2019) 12004.

[15] H. Wang, J.-F. Flor, Y. Sun, Y. Wu, Numerical investigations on the thermal performance of adaptive ETFE foil cushions, Energy Procedia 158 (2019) 3191–3195.

[16] J. Hu, W. Chen, B. Zhao, D. Yang, Buildings with ETFE foils: a review on material properties, architectural performance and structural behavior, Construct. Build. Mater. 131 (2017) 411–422.

[17] C. Maywald, F. Riesser, Sustainability – the art of modern architecture, Procedia Eng. 155 (2016) 238–248.

[18] C. Wieser, Luftkissenarchitektur : Geschäftshaus "La Miroiterie" in Lausanne von Brauen + Wälchli, Werk, Bauen + Wohnen 95 (2008) 30–35.

[19] C. Risen, Award: Dynamic ETFE Façade, Hanley Wood Media, Inc, Washington, DC, 2017.

[20] S. Tanno, ETFE foil cushions as an alternative to glass for atriums and rooflights, in: International Conference on Building, Envelope Systems and Technology, Bath, 1997.

[21] K. Moritz, R. Barthel, Bauen mit ETFE-Folien, in: DETAIL Praxis -Transluzente Materialien, Institut für Internationale Architekturdokumentation, München, 2003, pp. 70–78.

[22] A. Gómez-González, J. Neila, J. Monjo, Pneumatic skins in architecture. Sustainable trends in low positive pressure inflatable systems, Procedia Eng. 21 (2011) 125–132.

[23] G. Grunwald, Mechanisch Vorgespannte, Doppellagige Membranmodule in Ihrer Anwendung Als Zweite Gebäudehülle, 2007. Berlin.

[24] J. Ward, J.C. Chilton, A. Heslop, l. Rowell, Internal environment in ETFE foil covered building enclosures, in: TensiNet Symposium 2010 - Tensile Architecture: Connecting Past and Future, University of Architecture, Civil Engineering and Geodesy (UACEG), Sofia, Bulgaria, 2010.

[25] J. Cremers, Energy saving design of membrane building envelopes, in: Structural Members: International Conference on Textile Composites and Inflatable Structures, 2011. Barcelona.

[26] M.A. Shameri, M.A. Alghoul, K. Sopian, M.F.M. Zain, O. Elayeb, Perspectives of double skin façade systems in buildings and energy saving, Renew. Sustain. Energy Rev. 15 (2011) 1468–1475.

[27] A. Ghaffarianhoseini, A. Ghaffarianhoseini, U. Berardi, J. Tookey, D.H.W. Li, S. Kariminia, Exploring the advantages and challenges of double-skin façades (DSFs), Renew. Sustain. Energy Rev. 60 (2016) 1052–1065.

[28] H. Tang, T. Zhang, X. Liu, X. Liu, X. Xiang, Y. Jiang, On-site measured performance of a mechanically ventilated double ETFE cushion structure in an aquatics center, Sol. Energy 162 (2018) 289–299.

[29] G. Ciampi, Y. Spanodimitriou, M. Scorpio, A. Rosato, S. Sibilio, Energy performance of PVC-Coated polyester fabric as novel material for the building envelope: model validation and a refurbishment case study, J. Build. Eng. 41 (2021) 102437.

[30] A. Faramarzi, B. Stephens, M. Heidarinejad, Optimal control of switchable ethylene-tetrafluoroethylene (ETFE) cushions for building façades, Sol. Energy 218 (2021) 180–194.

[31] M. Kersken, Method for the climate-independent determination of the solar heat gain coefficient (SHGC; g-value) of transparent façade and membrane constructions from in situ measurements, Energy Build. 239 (2021) 110866.

[32] W. Zhao, W. He, Z. Hu, X. Zheng, S. Zhang, G. Xu, H. Chen, Y. Yuan, Daylight and Thermal Performance of a Switchable Ethylene Tetra-Fluoro-Ethylene Cushion with Dynamic Control in Different Climates, Building Simulation, 2021.

[33] C. Monticelli, S. Lombardi, C. Würfl, H. Mohamed Ibrahim, Ellipsoidal Shape and Daylighting Control for the ETFE Pneumatic Envelope of a Winter Garden, 2013.

[34] H.-J. Tantau, J. Hinken, B. von Elsner, J. Max, A. Ulbrich, U. Schurr, T. Hofmann, G. Reisinger, Solar transmittance of greenhouse covering materials, Acta Hortic. 956 (2012) 441–448, 10.

[35] D. Masih, B. Lau, The Investigation of the Luminous Environment in ETFE Structures, 2015.

[36] H.B. Liu, B. Li, Z.H. Chen, T. Zhou, Q. Zhang, Solar radiation properties of common membrane roofs used in building structures, Mater. Des. 105 (2016) 268–277.

[37] D. Uribe, W. Bustamante, S. Vera, Seasonal optimization of a fixed exterior complex fenestration system considering visual comfort and energy performance criteria, Energy Procedia 132 (2017) 490–495.

[38] A. Roy, H. Ullah, A. Ghosh, H. Baig, S. Sundaram, A.A. Tahir, T.K. Mallick, Understanding the semi-switchable thermochromic behavior of Mixed halide hybrid perovskite nanorods, J. Phys. Chem. C 125 (2021) 18058–18070.

[39] S. Nundy, A. Mesloub, B.M. Alsolami, A. Ghosh, Electrically actuated visible and near-infrared regulating switchable smart window for energy positive building: a review, J. Clean. Prod. 301 (2021) 126854.

[40] A. LeCuyer, ETFE. Technology and Design, Birkhauser Verlag AG, Basel, Switzerland, 2008.

[41] M. Roudsari Sadeghipour, A. Waelkens, A New Approach to Modeling Frit Patterns for Daylight, 2015.

[42] R. Mikkonen, S. Lahokallio, L. Frisk, M. Mäntysalo, Processing of Printed Silver Patterns on an ETFE Substrate, IEEE, 2018, pp. 1–7.

[43] J.-F. Flor, Y. Sun, P. Beccarelli, Y. Wu, J. Chilton, Switchable ETFE cushion: designing and building a model for experimental testing, in: IASS Annual Symposium 2019 – Structural Membranes 2019, 2019. Barcelona.

[44] M. Roudsari Sadeghipour, M. Pak, A. Smith, G.G. Architecture, Ladybug: a parametric environmental plugin for grasshopper to help designers create an environmentally-conscious design, in: 13th Conference of International Building Performance Simulation Association, Chambery, 2013.

[45] M. Roudsari Sadeghipour, in: Honeybee Primer, web ed., GitBook, 2020, p. 511. https://www.scribd.com/document/303440360/Honeybee-Primer.

[46] S. Subramaniam, Parametric Modeling Strategies for Efficient Annual Analysis of Daylight in Buildings, US, 2018.

[47] P. Bakmohammadi, E. Noorzai, Optimization of the design of the primary school classrooms in terms of energy and daylight performance considering occupants' thermal and visual comfort, Energy Rep. 6 (2020) 1590–1607.

[48] D.A.A. Masih, B. Lau, J. Chilton, Daylighting performance in an atrium with ETFE cushion roof and in an ETFE-encapsulated panel structure, in: 6th International Building Physics Conference (Ibpc 2015), vol. 78, 2015, pp. 483–488.

[49] B. Lau, D.A.A. Masih, A.A. Ademakinwa, S.W. Low, J. Chilton, Understanding light in lightweight fabric (ETFE foil) structures through field studies, Procedia Eng. 155 (2016) 479–485.

[50] P. Good, T. Cooper, M. Querci, N. Wiik, G. Ambrosetti, A. Steinfeld, Spectral reflectance, transmittance, and angular scattering of materials for solar concentrators, Sol. Energy Mater. Sol. Cells (2016) 509–522.

[51] J. Cremers, H. Marx, Improved daylight comfort by a new 3D-foil that allows to trade off solar gains and light individually, in: Structural Membranes 2017, 2017. Munich.

[52] X. Liu, Y. Wu, Monte-Carlo optical model coupled with Inverse Adding-Doubling for Building Integrated Photovoltaic smart window design and characterisation, Sol. Energy Mater. Sol. Cell. 223 (2021) 110972.

[53] ISO, ISO 9050:2003 Glass in Building — Determination of Light Transmittance, Solar Direct Transmittance, Total Solar Energy Transmittance, Ultraviolet Transmittance and Related Glazing Factors, 2003.

[54] E. C. f. Standardization, BS EN 410 Glass in Building - Determination of Luminous and Solar Characteristics of Glazing, CEN-CENELEC Management Centre BSI Standards Publication, Brussels, Belgium, 2011.

[55] B.P. Jelle, Solar radiation glazing factors for window panes, glass structures and electrochromic windows in buildings—measurement and calculation, Sol. Energy Mater. Sol. Cell. 116 (2013) 291–323.

[56] J. Knippers, J. Cremers, J. Lienhard, M. Gabler, Construction Manual for Polymers + Membranes, Birkhauser Verlag AG, Basel, 2011.

[57] S. Afrin, Thermal Performance Analysis of ETFE-Foil Panels and Spaces Enclosed with ETFE-Foil Cushion Envelope, 2016. Nottingham.

[58] C. Maywald, Coating of ETFE solar shading for architectural applications, in: The 6th International TensiNet Symposium " Softening the Habitats : Sustainable Innovations in Minimal Mass Structures and Lightweight Architectures", Politecnico di Milano, Milan, Italy, 2019.

[59] C. Kohler, Simulation of complex glazing products; from optical data measurements to model based predictive controls, in: BEST 3 Conference, 2012.

[60] G. D'Anza, Rhino membrane plug-in. http://www.ixray-ltd.com, 2020.

[61] K.-U. Bletzinger, E. Ramm, A general finite element approach to the form finding of tensile structures by the updated reference Strategy, Int. J. Space Struct. 14 (1999) 131–145.

[62] D. Veenendaal, P. Block, An overview and comparison of structural form finding methods for general networks, Int. J. Solid Struct. 49 (2012) 3741–3753.

[63] G.L. Ward, R. Shakespeare, Rendering with Radiance: the Art and Science of Lighting Visualization, Morgan Kaufmann Publishers Inc., 1998, p. 664.

[64] B.J. Lindbloom. http://www.brucelindbloom.com, 2020.

[65] C.F. Reinhart, M. Andersen, Development and validation of a Radiance model for a translucent panel, Energy Build. 38 (2006) 890–904.

[66] B. Deroisy, A. Deneyer, G. Lethé, G. Flamant, Bi-directional scattering distribution data of solar shading: characterization and performances, in: CIE Centenary Conference 2013, 2013. Paris.

[67] R. Capperucci, R.C.G.M. Loonen, J.L.M. Hensen, A.L.P. Rosemann, Angle-dependent optical properties of advanced fenestration systems—finding a right balance between model complexity and prediction error, Build. Simul. 12 (2019) 113–127.

[68] C. Asmail, Bidirectional scattering distribution function (BSDF): a systematized bibliography, J. Res. Nat. Inst. Stand. Technol. 96 (1991) 215–223.

[69] G. Ward, R. Mistrick, E.S. Lee, A. McNeil, J. Jonsson, Simulating the daylight performance of complex fenestration systems using bidirectional scattering distribution functions within radiance, Leukos 7 (2011) 241–261.

[70] A. McNeil, BSDFViewer: A Utility for Interactive Exploration of BSDF Datasets, 2013.

[71] G. Molina, W. Bustamante, J. Rao, P. Fazio, S. Vera, Evaluation of radiance's genBSDF capability to assess solar bidirectional properties of complex fenestration systems, J. Build. Perform. Simul. 8 (2015) 216–225.

[72] L.O. Grobe, A. Noback, S. Wittkopf, Z.T.ç. Kazanasmaz, Comparison of measured and computed BSDF of a daylight redirecting component, in: CISBAT 2015, 2015. Lausanne.

[73] A.G. Mainini, A. Zani, G. De Michele, A. Speroni, T. Poli, M. Zinzi, A. Gasparella, Daylighting Performance of Three-Dimensional Textiles, Energy and Buildings, 2019.

[74] D. Geisler-Moroder, E. Lee, G. Ward, B. Bueno, L.O. Grobe, T. Wang, B. Deroisy, H.R. Wilson, BSDF Generation Procedures for Daylighting Systems, 2021.

[75] L. Grobe, Irregular Light Scattering Properties of Innovative Fenestration for Comfortable and Energy-Efficient Buildings, 2020.

[76] M. Andersen, M. Rubin, R. Powles, J.L. Scartezzini, Bi-directional transmission properties of Venetian blinds: experimental assessment compared to ray-tracing calculations, Sol. Energy 78 (2005) 187–198.

[77] A. McNeil, C.J. Jonsson, D. Appelfeld, G. Ward, E.S. Lee, A validation of a ray-tracing tool used to generate bi-directional scattering distribution functions for complex fenestration systems, Sol. Energy 98 (2013) 404–414.

[78] G.J. Ward, T. Wang, D. Geisler-Moroder, E.S. Lee, L.O. Grobe, J. Wienold, J. C. Jonsson, Modeling specular transmission of complex fenestration systems with data-driven BSDFs, Build. Environ. (2021) 107774.

[79] J.H. Klems, A new method for predicting the solar heat gain of complex fenestration systems, Build. Eng. 100 (1994) 16.

[80] A. McNeil, The Three-phase Method for Simulating Complex Fenestration with Radiance, 2013.

[81] D. Geisler-Moroder, S.E. Lee, J.G. Ward, Validation of the Five-phase Method for Simulating Complex Fenestration Systems with Radiance against Field Measurements, 2018.

[82] A. Vlachokostas, N. Madamopoulos, Daylight and thermal harvesting performance evaluation of a liquid filled prismatic façade using the Radiance five-phase method and EnergyPlus, Build. Environ. 126 (2017) 396–409.

[83] E.S. Lee, D. Geisler-Moroder, G. Ward, in: L.B.N. Laboratory (Ed.), Validation of the Five-phase Method for Simulating Complex Fenestration Systems with Radiance against Field Measurements, Lawrence Berkeley National Laboratory, 2018. https://escholarship.org/uc/item/24h966pp.

[84] G. Ward, Computing and Applying Variable-Resolution Data for Bidirectional Scattering Distribution Functions, DOE/LBNL, Berkeley, 2011.

[85] A. McNeil, E.S. Lee, A validation of the Radiance three-phase simulation method for modelling annual daylight performance of optically complex fenestration systems, J. Build. Perform. Simul. 6 (2013) 24–37.

[86] C.F. Reinhart, S. Herkel, The simulation of annual daylight illuminance distributions — a state-of-the-art comparison of six RADIANCE-based methods, Energy Build. 32 (2000) 167–187.

[87] P.R. Tregenza, Uncertainty in daylight calculations, Light. Res. Technol. 49 (2016) 829–844.

[88] DIN, DIN EN 4543-1:1994-09 Office Work Place - Part 1: Space for the Arrangement and Use of Office Furniture; Safety Requirements, Testing, 1994.

[89] M. Qingsong, H. Fukuda, Parametric office building for daylight and energy analysis in the early design stages, in: Urban Planning and Architecture Design for Sustainable Development, UPADSD 2015, Lecce, 2015.

[90] T. Wang, G. Ward, E.S. Lee, Efficient modeling of optically-complex, non-coplanar exterior shading: validation of matrix algebraic methods, Energy Build. 174 (2018) 464–483.

[91] Y. Sun, Y. Wu, R. Wilson, Analysis of the daylight performance of a glazing system with ParallelSlat transparent insulation material (PS-TIM), Energy Build. (2017) 616–633.

[92] D.A. Chi, D. Moreno, J. Navarro, Impact of perforated solar screens on daylight availability and low energy use in offices, Adv. Build. Energy Res. 15 (2021) 117–141.

[93] BS EN 12464-1, 2011 - light and lighting. Lighting of work places, Indoor Work Places (2011).

[94] S. Olbina, J. Hu, Daylighting and thermal performance of automated split-controlled blinds, Build. Environ. 56 (2012) 127–138.

[95] K. Konis, E.S. Lee, Measured daylighting potential of a static optical louver system under real sun and sky conditions, Build. Environ. 92 (2015) 347–359.

[96] L. Santos, A. Leitão, L. Caldas, A comparison of two light-redirecting fenestration systems using a modified modeling technique for Radiance 3-phase method simulations, Sol. Energy 161 (2018) 47–63.

[97] Y. Fang, S. Cho, Design optimization of building geometry and fenestration for daylighting and energy performance, Sol. Energy 191 (2019) 7–18.

[98] A. Mkntaser Koohsari, S. Heidari, Optimizing Window Size by Integrating Energy and Lighting Analyses Considering Occupants' Visual Satisfaction, Built Environment Project and Asset Management, 2020, p. 11, ahead-of-print.

[99] Y. Sun, D. Liu, J.-F. Flor, K. Shank, H. Baig, R. Wilson, H. Liu, S. Sundaram, T. K. Mallick, Y. Wu, Analysis of the daylight performance of window integrated photovoltaics systems, Renew. Energy 145 (2020) 153–163.

[100] Z. Kong, J.A. Jakubiec, Evaluations of long-term lighting qualities for computer labs in Singapore, Build. Environ. (2021) 107689.

[101] A. Nabil, J. Mardaljevic, Useful daylight illuminances: a replacement for daylight factors, Energy Build. 38 (2006) 905–913.

[102] C. I., Chartered Institution of Building Services Engineers, Environmental Design : CIBSE Guide A, 2015. London, UK.

[103] CIE, in: 117-1995 Discomfort Glare in Interior Lighting, 3. CIE Technical Committee TC, 1995, p. 39.

[104] J. Wienold, J. Christoffersen, Evaluation methods and development of a new glare prediction model for daylight environments with the use of CCD cameras, Energy Build. 38 (2006) 743–757.

[105] J. Wienold, Dynamic daylight glare evaluation, in: Building Simulation 2009, the 11th International IBOSA Conference, 2009. Glasgow.

[106] S.A. Kleindienst, M. Andersen, The adaptation of daylight glare probability to dynamic metrics in a computational stting, in: 11th European Lighting Conference, Istanbul, 2009.

[107] J. Suk, M. Schiler, Investigation of Evalglare software, daylightglare probability and high dynamic rangeimaging for daylight glare analysis, Light. Res. Technol. 45 (2013) 450–463.

[108] I. Konstantzos, A. Tzempelikos, Y.-C. Chan, Experimental and simulation analysis of daylight glare probability in offices with dynamic window shades, Build. Environ. 87 (2015) 244–254.

[109] Q.-G. Deng, G.-Y. Cao, Z.-C. Liu, Z.-S. Wang, Y. Yang, X.-Y. He, J.-J. Yu, Annual daylight glare evaluation: impact of weather file selection, Light. Res. Technol. (2016) 446–455.
[110] A. Ghosh, B. Norton, A. Duffy, Daylighting performance and glare calculation of a suspended particle device switchable glazing, Sol. Energy 132 (2016) 114–128.
[111] A. Tzempelikos, Y.-C. Chan, Estimating detailed optical properties of window shades from basic available data and modeling implications on daylighting and visual comfort, Energy Build. 126 (2016) 396–407.
[112] J. Wienold, T. Kuhn, J. Christoffersen, M. Andersen, Annual Glare Evaluation for Fabrics, 2017.
[113] L. Giovannini, F. Favoino, V.R.M. Lo Verso, A. Pellegrino, V. Serra, A simplified approach for the annual and spatial evaluation of the comfort classes of daylight glare using vertical illuminances, Buildings 8 (2018) 171.
[114] J.Y. Suk, Luminance and vertical eye illuminance thresholds for occupants' visual comfort in daylit office environments, Build. Environ. 148 (2019) 107–115.
[115] E.F. Triantafyllidou, A.G. Michael, The impact of installing a concave curved profile blind to a glass window for visual comfort in office buildings, Procedia Manuf. 44 (2020) 269–276.
[116] L. Giovannini, F. Favoino, V.R.M. Lo Verso, V. Serra, A. Pellegrino, GLANCE (GLare ANnual Classes Evaluation): an approach for a simplified spatial glare evaluation, Build. Environ. 186 (2020) 107375.
[117] L. Santos, L. Caldas, Assessing the glare potential of side-lit indoor spaces: a simulation-based approach, Architect. Sci. Rev. 64 (2021) 139–152.
[118] A. Sepúlveda, B. Bueno, T. Wang, H.R. Wilson, Benchmark of methods for annual glare risk assessment, Build. Environ. 201 (2021) 108006.
[119] A. Eltaweel, Y. Su, Using integrated parametric control to achieve better daylighting uniformity in an office room: a multi-Step comparison study, Energy Build. 152 (2017) 137–148.
[120] C.T. Do, Y.-C. Chan, Daylighting performance analysis of a facade combining daylight-redirecting window film and automated roller shade, Build. Environ. 191 (2021) 107596.
[121] D. de Loyola Ramos Garcia, F.O.R. Pereira, Method application and analyses of visual and thermal-energy performance prediction in offices buildings with internal shading devices, Build. Environ. 198 (2021) 107912.
[122] J.-F. Flor, Switchable ETFE Façades: A Study on the Thermo-Optical, Daylighting and Energy Performance of Climate Adaptive Building Envelopes, 2021.
[123] https://energyplus.net/. (Accessed March 2018).